AEDC-TR-90-22

C#2

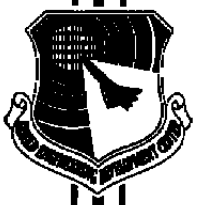

Development of a Free-Jet Forebody Simulator Design Optimization Method

D. R. Huddleston
Sverdrup Technology, Inc./AEDC Group

December 1990

Final Report for Period October 1, 1988 through June 30, 1990

ARNOLD ENGINEERING DEVELOPMENT CENTER
ARNOLD AIR FORCE BASE, TENNESSEE
AIR FORCE SYSTEMS COMMAND
UNITED STATES AIR FORCE

NOTICES

When U. S. Government drawings, specifications, or other data are used for any purpose other than a definitely related Government procurement operation, the Government thereby incurs no responsibility nor any obligation whatsoever, and the fact that the Government may have formulated, furnished, or in any way supplied the said drawings, specifications, or other data, is not to be regarded by implication or otherwise, or in any manner licensing the holder or any other person or corporation, or conveying any rights or permission to manufacture, use, or sell any patented invention that may in any way be related thereto.

Qualified users may obtain copies of this report from the Defense Technical Information Center.

References to named commercial products in this report are not to be considered in any sense as an endorsement of the product by the United States Air Force or the Government.

This report has been reviewed by the Office of Public Affairs (PA) and is releasable to the National Technical Information Service (NTIS). At NTIS, it will be available to the general public, including foreign nations.

APPROVAL STATEMENT

This report has been reviewed and approved

Mark S. Briski

MARK S. BRISKI, Capt, USAF
Directorate of Technology
Deputy for Operations

Approved for publication:

FOR THE COMMANDER

Keith L. Kushman

KEITH L. KUSHMAN
Technical Director
Directorate of Technology
Deputy for Operations

REPORT DOCUMENTATION PAGE

Form Approved
OMB No. 0704-0188

1 AGENCY USE ONLY (Leave blank)	2 REPORT DATE	3 REPORT TYPE AND DATES COVERED
	December 1990	Final, October 1, 1988 - June 30, 1990

4 TITLE AND SUBTITLE
Development of a Free-Jet Forebody Simulator Design Optimization Method

5 FUNDING NUMBERS
PE-65807F

6 AUTHOR(S)
Huddleston, David H.,Sverdrup Technology, Inc./AEDC Group

7 PERFORMING ORGANIZATION NAME(S) AND ADDRESS(ES)
Arnold Engineering Development Center/DOT
Air Force Systems Command
Arnold Air Force Base, TN 37389-5000

8. PERFORMING ORGANIZATION REPORT NUMBER
AEDC-TR-90-22

9 SPONSORING/MONITORING AGENCY NAMES(S) AND ADDRESS(ES)
Arnold Engineering Development Center/DO
Air Force Systems Command
Arnold Air Force Base, TN 37389-5000

10. SPONSORING/MONITORING AGENCY REPORT NUMBER

11 SUPPLEMENTARY NOTES
Available in Defense Technical Information Center (DTIC).

12a. DISTRIBUTION/AVAILABILITY STATEMENT
Approved for public release; distribution is unlimited.

12b. DISTRIBUTION CODE

13 ABSTRACT (Maximum 200 words)
An aerodynamic design optimization technique is presented that couples direct optimization algorithms with the analysis capability provided by appropriate computational fluid dynamics (CFD) programs. This technique is intended to be an aid in designing the aerodynamic shapes and establishing test conditions required for the successful simulation of aircraft engine inlet conditions in a ground test environment. However, the method is also applicable to other aerodynamic design problems such as airfoil design, turbomachinery cascade design, and nozzle design. The approach involves minimization of a nonlinear least-squares objective function that may be defined in a region remote to the geometric surface being optimized. In this study, finite-difference Euler and Navier-Stokes codes were applied to obtain the objective function evaluations, although the applied optimization method can be coupled with any appropriate CFD analysis technique. Using CFD to compute design space gradients within an optimization algorithm has received little prior attention in the literature. It is demonstrated, herein, that CFD can be used in this manner by applying the developed design technique to a variety of aerodynamic design problems. Results are presented for several typical aerospace examples, including inviscid and viscous flow over airfoils, flows in convergent/divergent nozzles in both two and three dimensions, and supersonic flow about a planar forebody simulator.

14. SUBJECT TERMS	15. NUMBER OF PAGES
aerodynamic design optimization **design by analysis** **nonlinear optimization** **direct optimization methods**	**78** 16. PRICE CODE

17 SECURITY CLASSIFICATION OF REPORT	18 SECURITY CLASSIFICATION OF THIS PAGE	19. SECURITY CLASSIFICATION OF ABSTRACT	20. LIMITATION OF ABSTRACT
UNCLASSIFIED	**UNCLASSIFIED**	**UNCLASSIFIED**	**SAME AS REPORT**

COMPUTER GENERATED

Standard Form 298 (Rev. 2-89)
Prescribed by ANSI Std. Z39-18
298-102

PREFACE

The work reported herein was conducted by the Arnold Engineering Development Center (AEDC), Air Force Systems Command (AFSC). The results of the research were obtained by Sverdrup Technology, Inc., AEDC Group (a Sverdrup Corporation Company), operating contractor for the propulsion test facilities at AEDC, AFSC, Arnold Air Force Base, Tennessee 37389, under Project Number DB84EW. The Air Force Project Manager was Capt. Mark Briski, DOT. This portion of the research was completed on June 30, 1990, and the manuscript was submitted for publication on November 7, 1990.

CONTENTS

ILLUSTRATIONS

Figure Page

Figure Page

Figure Page

APPENDIXES

1.0 INTRODUCTION

The ambitious operating envelopes desired for future fighter aircraft dictates an aircraft industry requirement to test integrated propulsion system components at a ground test facility. In response to this industry need, the Arnold Engineering Development Center (AEDC) is developing an extensive free-jet test capability for this application (Ref. 1). One factor that inhibits the utilization of free-jet testing capability at the AEDC is the reliance upon empirical techniques for the design of the forebody simulator used to tailor the flow field to the desired flight conditions. To alleviate this deficiency, the joint ASD/AEDC Aeropropulsion System Test Facility (ASTF) free-jet development technical steering committee proposed development of an aerodynamic design optimization capability applicable to the forebody simulator design problem. This capability, referred to as the "generation 6" design method within the joint ASD/AEDC ASTF free-jet development plan, was intended to combine nonlinear optimization methods with the powerful analysis capability afforded by computational fluid dynamics (CFD). Application of Euler or Navier-Stokes CFD analysis codes within the design optimization is motivated by the aerodynamic complexity of typical free-jet test configurations. The objective of this report is to document the progress that has been made to date toward development of such an aerodynamic design optimization capability.

A schematic of the forebody simulator design optimization problem is illustrated in Fig. 1. This figure depicts a free-jet inlet-engine test configuration within a generic ground test facility designed to evaluate the performance of an integrated propulsion system. The design requirement is to produce a flow field across a specified inlet reference plane in the free-jet installation that is similar, within a predefined tolerance, to that which would be encountered in flight. One proposed way of achieving this is by appropriately designing a "flow-tailoring" forebody simulator, and/or varying free-jet flow conditions (total pressure, total temperature, flow angle, and Mach number) to produce the desired flow field at the inlet reference plane (Ref. 1). The plane where fluid dynamic similarity is required will hereafter be referred to as the inlet reference plane (IRP). The fundamental assumption of this free-jet test concept is that adequate similitude is attained whenever the fluid dynamic state at the indicated reference plane adequately matches that which is specified for a given operating condition.

The task of designing such a flow-tailoring geometry and the corresponding test conditions is formidable. The test designer must specify a forebody simulator geometry and free-jet fluid properties that produce, within design tolerance, the desired fluid dynamic state at the region of interest. Current forebody simulator design methods rely heavily upon prior experience to guide a trial-and-error design approach using subscale testing and CFD analyses to evaluate the candidate designs. This process is inefficient and does not ensure an orderly progression toward an acceptable design. Thus, the specific purpose of the research reported herein was to develop a reliable method, based upon CFD analyses, for the specification

of an acceptable set of aerodynamic design parameters (both geometric and fluid dynamic) for complex designs typical of those encountered in an aerodynamic test facility. The ultimate goal of the research is to optimize the design of a complex three-dimensional (3-D) configuration, such as illustrated in Fig. 1, in a timely and cost-effective manner. Development of such a design optimization method very obviously requires the ability to perform an accurate CFD analysis of the proposed design. However, the evaluation of various CFD techniques, relative to simulation of typical free-jet testing configurations, is not reported. The CFD evaluation effort is being conducted in parallel with the design optimization development and is reported in AEDC-TR-90-21 by M. D. McClure and J. R. Sirbaugh (to be published).

As an optimization problem, a forebody simulator design possesses several interesting features in that (1) the flow-field constraints are imposed at a location away from the geometric surface that is being optimized; (2) both fluid dynamic and geometric design variables must be optimized; (3) discontinuous or localized high-gradient behavior may occur within the design space (e.g., shocks or onset of separated flow); and (4) an extensive history of prior, similar designs does not exist. Characteristics (1) and (2) do not constitute a well-posed inverse design problem; however, the imposition of flow-field data, in the described manner, does properly define a direct optimization problem. Since flow-field data are prescribed at a known reference plane, it is possible to define an objective function that measures a norm between the reference plane flow properties associated with a particular design point (set of independent design variable values) and the desired reference plane flow properties. Since the norm is a function of the given design variables, the optimization task is to determine the particular values of these variables that produce a minimum value for the objective function. This is accomplished by optimizing the selected design parameters through the minimization of a nonlinear least-squares objective function. Flexibility in the type of designs that can be considered is provided through the use of modern CFD codes to produce the function evaluations required by the optimization algorithm. The resulting direct optimization approach is applicable in both two and three dimensions, and in principle, any CFD technique appropriate to the flow regime of interest could be used.

Using an Euler or Navier-Stokes CFD code to compute design space gradients within an optimization algorithm has received little prior attention in the literature. It is demonstrated that this can be accomplished by applying the developed design technique to a variety of aerodynamic design problems. The test problems were constructed to illustrate the applicability of this approach to realistic designs by deliberately selecting poor initial conditions for the optimization algorithm. The aerodynamic optimization examples presented include a NACA0012 airfoil, convergent/divergent nozzles, and a planar supersonic forebody simulator. Although the method applied is applicable to either viscous or inviscid flows, only one viscous example is presented because of the increased computational expense required for a viscous CFD analysis.

This report is organized so that the design optimization technique is developed and presented in Section 2. The design technique is demonstrated by application to several aerodynamic examples in Section 3. Comments relevant to the application of this technique, in its present state of development, are presented in Section 4. Lastly, some conclusions relative to design optimization using the developed technique and some recommendations for future research are presented in Sections 5 and 6.

2.0 NUMERICAL TECHNIQUE

Using CFD to optimize aerodynamic designs is currently an active research topic in the applied mathematics and engineering disciplines. The motivation for developing and using these optimization methods in the design process is to reduce the overall computational effort needed to develop aerodynamic components and configurations, which will optimize a selected measure of aerodynamic performance. Several examples of aerodynamic design optimizations exist in recent literature, such as the design of airfoils, turbomachinery cascades, ducts, and nozzles. A brief literature survey was provided by the author (Ref. 2) and is not repeated herein. However, it is noteworthy that similar direct optimization methods have previously been coupled with method-of-characteristics flow solvers at the AEDC by Varner (Ref. 3) and F. L. Shope (unpublished work). Additionally, a similar development project has been proposed recently for application to the design of hypersonic nozzle contours by P. F. Hoffman (unpublished work).

2.1 BACKGROUND

The implementation of optimized aerodynamic design generally follows one of three approaches: (1) inverse design methods, (2) basis function optimization methods, and (3) direct function optimization methods. Generally, true inverse design methods are more efficient than either the basis function approach or direct optimization since the determination of the optimal design is made as an integral part of the CFD analysis. However, since many aerodynamic design problems cannot be cast in an inverse form, direct optimization methods and basis function methods are often applied.

An application such as the free-jet forebody simulator illustrated in Fig. 1, is too general for successful application of either a classic inverse method or the basis function approach. However, almost any design problem can be cast as a direct function optimization if a tangible measure of the design's quality can be identified to define an objective function that is responsive to changes in the selected design parameters. Thus, the implementation of a direct aerodynamic optimization technique is investigated and reported herein as well as in Refs. 2, 4, and 5. It is recognized that the penalty for this generality is a potentially less efficient optimization method for some of the simpler applications that may be of interest such as airfoils and supersonic nozzles.

With current computer technology and CFD algorithms, many complex two-dimensional (2-D) and some 3-D aerodynamic designs can be adequately analyzed, although the computational cost can be very high. Applying an optimization method that uses CFD to provide function evaluations will be computationally expensive since multiple CFD analyses are required. Even so, for problems such as the previously described forebody simulator, some form of design optimization is required because the cost of the available alternatives (e.g., experimental "cut and try" in a wind tunnel using an inlet/forebody simulator model) may be even more prohibitive. Additionally, investigation of a more general aerodynamic design optimization technique will help prepare the way for future enhancements as computer hardware, CFD algorithms, and optimization algorithms become more efficient.

Within this research, the direct optimization problem was formulated as a nonlinear least-squares minimization using existing CFD analysis codes to provide the function evaluations required by the optimization algorithm. Both Gauss-Newton and quasi-Newton optimization algorithms were applied to minimize the least-squares objective function. The optimization algorithms were coupled with the CFD analysis code as illustrated in Fig. 2 to yield the desired interaction between the CFD analysis capability and the design optimization algorithm. The optimization code was kept distinct from the CFD analysis code to provide the analyst with the flexibility to select the most appropriate CFD analysis technique for a given design problem.

Implementation of this optimization technique involved three primary problems, (1) method of function evaluation, (2) selection of the objective function and implementation of the optimization algorithm, and (3) specification of the design parameters. Each of these items is discussed in the remainder of this section.

2.2 OBJECTIVE FUNCTION EVALUATION

In selecting the type of CFD analysis to use in evaluating the objective function, the anticipated flow regime to be encountered computationally was identified (Ref. 1). A typical free-jet test envelope can range from low subsonic flow to moderately high supersonic flows, potentially with the free-jet nozzle inclined at high angles of attack relative to the test article. The appropriate aerodynamic analysis for the motivating problem requires a complex, 3-D, flow-field computation, necessitating the application of an Euler code or a Navier-Stokes code to produce an accurate simulation. However, during a preliminary design phase, less accurate but more efficient CFD techniques may be used. By formulating the optimization problem as a nonlinear least-squares minimization, the particular flow-field analysis technique applied is irrelevant to the construction of the optimization algorithm as long as consistent and repeatable function evaluations are obtained. The flow-field simulation must be consistent and repeatable in the sense that small perturbations to design parameters are accurately reflected in the flow-field solution. This is important because the implemented optimization

algorithm uses these function evaluations to compute design space gradients. If these gradients are inaccurate, then obviously the algorithm would not converge to the correct solution.

Although the direct optimization design method can be coupled with any CFD technique appropriate to the problem of interest, the complexity of the forebody simulator design problem makes it necessary to demonstrate that the direct optimization technique can be coupled with an Euler or Navier-Stokes solver. Thus, within this report all of the CFD analyses were made using PARC, a general purpose, finite difference Euler/Navier-Stokes CFD code (Ref. 6). The version of this CFD code applicable to axisymmetric and 2-D configurations is referred to as PARC2D. The analogous 3-D CFD code is referred to as PARC3D. The PARC codes have been applied at the AEDC and elsewhere to analyze a variety of complex internal and external fluid mechanics problems (Refs. 7 through 10). This particular CFD code was selected because of its robustness, ease of use, and reliability. It produces consistent and repeatable flow simulations in the sense that small perturbations to design parameters are accurately reflected in the flow solution. All of the 2-D computational grids used were generated by the application of the INGRID code developed by Soni (Ref. 11).

The purpose of this research was not to demonstrate how well the PARC Euler/Navier-Stokes code can simulate a particular aerodynamic phenomenon or to improve the CFD analysis capability per se, but to demonstrate that an Euler/Navier-Stokes code can be coupled with efficient optimization methods to produce a potentially viable technique for optimizing aerodynamic designs that may be too complex to design by other available means. In the aerodynamic examples presented, no effort was made to obtain the most accurate CFD simulation for the given configuration. Whenever possible, a minimum number of grid points were applied to reduce computation time. No studies were made, for example, to assess effects of grid distribution on the CFD simulation. However, it was necessary to monitor the level of convergence, particularly at the reference plane, of each simulation used. It was necessary to reduce the temporal variation of flow variables at the reference plane, and this was accomplished by iterating on the flow field until the norm of the conservation variables at the reference plane was relatively stationary, typically to eight significant figures. To compute accurate design space gradients at the reference plane, the dominant change in the residual must be attributable to the change in the design parameters, and not transient effects. Demonstrating that CFD can be used, as described, within an optimization algorithm for aerodynamically complex configurations will extend current capabilities in aerodynamic design optimization.

2.3 OPTIMIZATION ALGORITHM

In the motivating design problem, the desired fluid dynamic state is completely known at the reference plane, either from experiment or free-stream CFD computation. The design

requirement is to minimize the error norm between these quantities and corresponding values computed for a particular design point. The norm was selected to be an L_2 norm of the difference between the target flow-field variables and the values computed for a given design point. The nonlinear least-squares form was selected because (1) the method is very versatile; (2) extensive literature is available on general nonlinear least-squares minimization; and (3) efficient Gauss-Newton and quasi-Newton methods are well documented for the nonlinear least-squares problem.

The nonlinear least-squares minimization was formulated as follows: Let the residuals $r_i(P_1,\ldots,P_M)$, $i=1,2,\ldots,N$, be functions of M design parameters,

$$r_i(P_1,P_2,\ldots,P_M) = y_i - f_i(P_1,P_2,\ldots,P_M) \tag{1}$$

where r_i denotes the difference between the N specified reference plane quantities, y_i, and the corresponding N quantities associated with the M parameters, f_i. The design parameters may be geometric, fluid dynamic, or both. To minimize r_i, in the least-squares sense, values for the parameters, P_j, are found that minimize

$$F(P_1,P_2,\ldots P_M) = \sum_{i=1}^{N} \{r_i(P_1,P_2,\ldots,P_M)\}^2 \tag{2}$$

where F is the objective function. This sum can be written in vector form as $\underline{R}(\underline{P})^T\underline{R}(\underline{P})$, where $\underline{P}$ denotes a vector with components P_i and $\underline{R}(\underline{P})$ denotes a vector of functions with components $r_i(\underline{P})$.

Three alternative sets of fluid dynamic variables were considered to specify the reference plane state including, (1) the Navier-Stokes dependent variables in conservation form, (2) the Navier-Stokes dependent variables in nonconservation form, and (3) RP total conditions and directional Mach number. Preliminary studies conducted in this research using a simple airfoil optimization problem detected no significant difference in results caused by the choice of dependent variables.

Except when otherwise noted, the set of variables used herein to define the reference plane (RP) fluid state are (1) RP total pressure, $P_{T_{rp}}$, (2) RP total temperature, $T_{T_{rp}}$, and (3) RP directional Mach number, $M_{x_{rp}}$, $M_{y_{rp}}$, and $M_{z_{rp}}$. In two dimensions, one less Mach number component is required. Variable constraints, when applied, are imposed by adding a barrier function, such as the inverse function (Ref. 12) to the objective function. Thus, the expression $\underline{R}^T\underline{R}$ becomes

$$\underline{R}^T\underline{R} = \sum_{i=1}^{N_r} \{(P_{T_{rp}} - P_T)_i^2 + (T_{T_{rp}} - T_T)_i^2 + (M_{x_{rp}} - M_x)_i^2 + (M_{y_{rp}} - M_y)_i^2 + (M_{z_{rp}} - M_z)_i^2\} \tag{3}$$

where N_r is the number of reference plane points. Since each term in Eq. (3) contains five residual fluid dynamic components, in order to put this in the form of Eq. (2), $N = 5N_r$ must hold. In Eq. (3) the subscript rp denotes the specified reference plane values, and unsubscripted values denote reference plane values computed for a particular trial design (set of design parameters). Quantities in Eq. (3) are normalized by appropriate reference quantities to produce target reference plane values of order one.

A popular and efficient algorithm for minimizing the nonlinear least-squares form, Eq. (1), is the Gauss-Newton method (Ref. 12) or one of its variants such as Hartley's modified Gauss-Newton method (Ref. 13). An advantage of these algorithms as applied to the least-squares form is the elimination of the need for the Hessian matrix in the algorithm formulation. Formation of the Hessian matrix requires specification and evaluation of $N \times M \times (M + 1)/2$ second derivative terms. For the motivating application, computation of the Hessian matrix is prohibitively expensive because these derivatives must be approximated by finite differences. Derivation of the Gauss-Newton method, applied to the least-squares problem, is available from several sources (Refs. 12 and 13) but is repeated in Appendix A.

Applying the Gauss-Newton method to minimize Eq. (1) yields an optimization algorithm of the form

$$J^T J \Delta \underline{P} = -J^T \underline{R} \tag{4}$$

where J denotes the Jacobian of $\underline{R}$ with respect to $\underline{P}$ defined by

$$J = \begin{pmatrix} \frac{\partial r_1}{\partial P_1} & \cdots & \frac{\partial r_1}{\partial P_M} \\ \vdots & & \vdots \\ \frac{\partial r_N}{\partial P_1} & \cdots & \frac{\partial r_N}{\partial P_M} \end{pmatrix} \tag{5}$$

Equation (4) defines an M-by-M system of equations that was used to compute the change, $\Delta \underline{P}$, in the design parameter solution vector, $\underline{P}$. To apply this algorithm, J was evaluated by finite difference approximation to obtain the partial derivative of each residual component with respect to each design parameter. This requires $M + 1$ function evaluations to compute the M partials for each residual. Since a CFD solution was used to obtain each function evaluation, approximation of this Jacobian was by far the most expensive part of the algorithm.

An extension of this algorithm is Broyden's quasi-Newton method (Refs. 12 and 14). Broyden's extension modifies the standard Gauss-Newton method by approximating the

Jacobian, J, at the k + 1 iteration strictly from the Jacobian and other data available at iteration k rather than recomputing J directly. Since, in quasi-Newton algorithms, a finite difference approximation to J is made only for the initial iteration, the accuracy of this approximation is even more important than for the Gauss-Newton technique. If the quasi-Newton algorithm is to converge to the optimal solution, an accurate initial approximation to J must be made. Applying Broyden's quasi-Newton method yields an optimization algorithm identical in form with the Gauss-Newton method, Eq. (4), and is given by

$$B^T B\Delta\underline{P} = -B^T \underline{R} \tag{6}$$

where the Jacobian approximation, B_k at iteration k, is updated for iteration k + 1 according to

$$B_{k+1} = B_k + \frac{(\Delta\underline{R}_k - B_k\Delta\underline{P}_k)\,\Delta\underline{P}_k^T}{(\Delta\underline{P}_k^T\,\Delta\underline{P}_k)} \tag{7}$$

where B_0 is obtained by a finite difference approximation to the Jacobian. This modification to the Gauss-Newton algorithm is based upon the Jacobian approximation developed by Broyden (Ref. 14), the derivation of which is repeated in Appendix B. One of the key assumptions used to derive Eq. (7) is that the residual change in directions orthogonal to the direction $\Delta\underline{P}_k$ predicted by B_{k+1} is identical to that predicted by B_k. The imposition of the quasi-Newton condition, which constrains B_{k+1} to hold exact derivative information in the direction of $\Delta\underline{P}_k$ for linear $\underline{R}$, provides the other conditions necessary to uniquely determine B_{k+1}. Application of the Gauss-Newton algorithm requires M + 1 function evaluations for each iteration since the Jacobian is approximated by finite differences, whereas Broyden's extension requires M + 1 function evaluations for the first iteration but only one evaluation for subsequent iterations. Thus, if the quasi-Newton method can be applied, after the first iteration, M function evaluations are eliminated at each iteration. For typical aerodynamic optimization problems, the function evaluation is the dominant part of the cost, and a significant savings is realized whenever the quasi-Newton algorithm can be applied.

It is well known that the Gauss-Newton method, using analytical derivatives, determines a search direction that guarantees a reduction in the objective function for some step size in that search direction (Ref. 13). Thus, a linear search technique is often employed once the search direction is determined by either the Gauss-Newton or quasi-Newton algorithm. The greatest benefit is derived from the linear search whenever the full correction computed by the optimization algorithm fails to produce a reduction in the objective function value. Because of the expense of function evaluations, a comparatively simple method, following Hartley (Ref. 13), was applied herein. When applying Hartley's technique, one function evaluation, in addition to the evaluation at the predicted optimum, was made in the determined

search direction. The base design point and the two new design points along the search direction were then used to define a quadratic interpolation function that was analytically solved to yield the optimal design parameters within the search interval.

The linear search adds at least one additional function evaluation per iteration. Because of the expense of function evaluations, the linear search was employed only when a full optimization step failed to produce a reduction in the objective function. The linear search strategy is described more fully in Appendix C.

2.4 DESIGN PARAMETERS

For the problem of interest, pertinent design variables are the free-jet fluid dynamic parameters and the variable forebody simulator geometry. The free-jet fluid dynamic parameters are specified as jet total pressure, jet total temperature, and jet Mach number. To produce an efficient optimization method, the forebody simulator geometry was described parametrically to reduce the total number of design variables. For two-dimensional applications, a parametric polynomial representation of 2-D curves as given by the Bernstein-Bezier polynomial (Ref. 15) was applied as follows:

$$\underline{x}(u) = \sum_{i=0}^{n} \frac{n!}{(n-i)!i!} u^i(1-u)^{(n-i)} \underline{x}_i;\ 0 \le u \le 1 \tag{8}$$

where $\underline{x}_0, \underline{x}_1, \underline{x}_2, \ldots, \underline{x}_n$ denote the position vectors of the n+1 geometric control points. In this form, the defined curve passes identically through the control points defined by vectors $\underline{x}_0$ and $\underline{x}_n$ but not through the remaining control points. This allows a high degree of variability for a given number of design parameters relative to other parametric representations with the penalty of making the influence of each parameter upon the total curve somewhat obscure. Application of the Bezier polynomials prevents the large oscillations encountered when using interpolating polynomials because of the "convex hull" property of Bezier polynomials. This property ensures that the Bezier polynomial lies within the polygon formed by connecting the vertices of each of the Bezier control vectors.

For 3-D applications, an extension of Eq. (8) defining Bezier surfaces (Ref. 15) was applied. The Bezier surfaces and interior were defined as follows:

$$\underline{x}(u,v,w) = \sum_{i=0}^{p} \sum_{j=0}^{q} \sum_{k=0}^{r} g_i^p(u)\, g_j^q(v)\, g_k^r(w)\, \underline{x}_{ijk} \tag{9}$$

Here $\underline{x}_{ijk}$ denotes the position vectors of the control points, $g_i^p(u)$, $g_j^q(v)$, and $g_k^r(w)$ are Bernstein basis functions of degree p,q, and r, respectively, and u,v, and w are parameters that range from 0 to 1. The Bernstein basis functions, $g_i^p(u)$, are defined by

$$g_i^p(u) = \frac{p!}{(p-i)!i!} u^i (1-u)^{(p-i)}; \; i = 0,1,2,\ldots p \qquad (10)$$

with the other basis functions analogously defined.

The set of design variables are of diverse type, including both geometric parameters and fluid dynamic parameters. Thus, each variable was nondimensionalized by an appropriate reference quantity. The nondimensionalization was chosen to make each design variable nominally of order one.

3.0 NUMERICAL EXAMPLES

The aerodynamic design optimization technique was evaluated by optimizing a series of numerical examples including, (1) algebraic test functions, (2) a NACA0012 airfoil in inviscid flow, (3) a NACA0012 airfoil in viscous flow, (4) a planar inviscid flow in a convergent/divergent nozzle, (5) a 3-D inviscid flow in a nozzle, and (6) an inviscid supersonic flow past a planar, forebody simulator. In each of these examples, the optimization problem was formulated so that a global minimum exists within the solution space. The evaluation criterion was to quantify the number of function evaluations required to determine the optimum.

The primary goal of this research was to demonstrate the feasibility of coupling CFD analyses capability with nonlinear optimization methods to produce an aerodynamic design technique. However, if the developed design method is to be successfully applied, it must also be efficient. For the subject application, efficiency can be equated with minimizing the total number of function evaluations required to isolate the optimum since this is where the preponderance of the computational cost is incurred. In fact, typical computer times required to evaluate the objective function, using an Euler or Navier-Stokes solver on a supercomputer, may range from several computer minutes for a simple 2-D design to many computer hours for a complex 3-D design with large amounts of computer memory required. The optimization algorithm applied, which used the function evaluations, typically executed in 5 to 10 sec on a CRAY® XMP supercomputer. The number of function evaluations was minimized by selecting an efficient optimization algorithm and applying an effective geometric parameterization to reduce the number of design variables.

Madabhushi, Levy, and Pincus (Ref. 16) developed a coupled direct optimization/CFD design method in which an objective function, defined as the average duct total pressure loss, was minimized as a general nonlinear function. The function minimizations were made by applying the Broyden, Fletcher, Goldfarb, and Shanno (BFGS) quasi-Newton algorithm. The selection of this quasi-Newton algorithm was based, in part, upon a comparison of the

relative performance of the BFGS algorithm, a conjugate gradient algorithm, and a gradient algorithm as applied to the minimization of ten algebraic test functions. The relative performance of the algorithms was measured by comparing the total number of function evaluations required for each method to converge to the global minimum. A disadvantage of the BFGS algorithm, relative to forebody simulator optimization, is the necessity to compute the design space Hessian matrix (matrix of second partial derivatives). Since these derivatives are not available analytically, computation of the Hessian represents both an expensive computation and a potentially unreliable computation because of potential inaccuracy in the objective function evaluation.

Several analytic test functions were used by the author (Ref. 2) to compare the relative efficiency of the Gauss-Newton algorithm and Broyden's quasi-Newton algorithm, as applied to the nonlinear least-squares minimization problem, with the results of Madabhushi et al. The goal of this comparison was to demonstrate that the optimization technique applied is reasonably efficient relative to other available optimization algorithms. If the comparisons are favorable, then the ease of application and versatility afforded by the nonlinear least-squares formulation makes this an attractive technique for application to aerodynamic design optimization. Reiterating a further advantage of the least-squares form applied herein is the elimination of the computation of the design space Hessian matrix. Generally, the results of the comparisons were favorable with the advantage of utilization of a less complex optimization algorithm. Specific details are given in Ref. 2.

3.1 INVISCID FLOW ABOUT A PLANAR AIRFOIL

Optimization of a planar airfoil in inviscid flow by specifying "reference plane" (RP) values at a station downstream of a NACA0012 airfoil (Fig. 3) provides an illustration of the design optimization technique. The RP was located at a vertical plane beginning at the airfoil trailing edge and extending five chord lengths into the computational domain. The NACA0012 airfoil is a well-known airfoil contour that has been extensively analyzed and is defined by

$$y(x) = 5t(0.2969x^{1/2} - 0.126x - 0.3516x^2 + 0.2843x^3 - 0.1015x^4) \qquad (11)$$

where the parameter, t, specifies the airfoil thickness. For the NACA0012 airfoil, the thickness parameter is specified as 0.12 for a chord length of 1.0089. This airfoil contour provided a convenient definition of a one-parameter design optimization problem for which the CFD analysis was very simple. The purpose of this example was to provide an aerodynamically simple design problem to demonstrate that it is possible to optimize an aerodynamic surface by specifying the fluid dynamic state at an RP remote to that surface.

The PARC2D CFD code was used to define the target RP properties by computing the inviscid flow field about this airfoil, subject to the boundary conditions indicated in Fig. 3. Nine thousand grid points were used to resolve the domain. Free-stream properties were held constant at a Mach number of 0.8 a distance of five to ten chord lengths away from the airfoil surface. Static pressure corresponding to the specified free-stream Mach number was specified at the indicated computational exit plane. The RP was located at the airfoil trailing edge and extended to the boundary of the computational domain. The influence of the body was shown to be minimal at approximately two chord lengths into the domain. The RP properties used to form the nonlinear least-squares objective function, as defined by Eq. (2), were minimized by application of Broyden's algorithm.

No effort was made to obtain a highly accurate CFD simulation. However, each simulation was scrutinized to assure that the solution, particularly at the RP, was strongly converged. In this example, each PARC2D solution was converged until the norm of the RP conservation variables was constant to eight significant figures. For this simple problem, the CFD results were consistent with those obtained by Jameson and Mavriplis (Ref. 17), among others, as evidenced by the pressure coefficient distribution along the airfoil surface (Fig. 4).

To initialize the optimization, the airfoil thickness was arbitrarily perturbed to 1/12 of its original value as an initial guess. This produced a very flat airfoil, which was obviously distinct from the target profile and thus produced a significant perturbation at the RP. In fact, as seen from the surface pressure profile (Fig. 4), the target airfoil is mildly transonic with a weak shock appearing at approximately midchord on the airfoil surface. Conversely, the almost flat profile used for an initial guess produced very little distortion of the free-stream with the flow field remaining subsonic throughout the domain.

The optimal design parameter was derived by applying Broyden's quasi-Newton algorithm. For the first iteration, the Jacobian, J, was approximated by a one-sided finite difference of each of the N residuals. This difference approximation is illustrated in the following example for the partial derivative of the i^{th} residual with respect to the design parameter, t,

$$\frac{\partial r_i}{\partial t} = \frac{r_i(t+\Delta t) - r_i(t)}{\Delta t} \tag{12}$$

Since a quasi-Newton algorithm was applied, a good approximation to the design space Jacobian was required at the first iteration. This Jacobian was not recomputed at subsequent iterations but was updated approximately according to Eq. (7).

To give an indication of the accuracy of this Jacobian, and to illustrate that stable computation of derivatives was possible for this problem, an investigation of derivative

accuracy versus the size of Δt used in Eq. (12) was performed. Figure 5 shows the variation of the normalized objective function derivative with respect to the design parameter versus the log of the parameter step size for first-order forward differences as given by Eq. (12). This gradient of the objective function was used to provide a crude assessment of the partial derivatives of the residual components that were used in the optimization algorithm. Although this does not provide detailed information about variation of individual residual derivatives, it does provide a means of measuring global variation at the RP. As can be seen, this derivative was sensitive to step size, but approached a constant value for step sizes less than 0.001. In fact, the actual data indicated that the derivative was constant within 0.5 of 1 percent for step sizes less than 0.001. Based upon this analysis, a step size of 0.001 was selected for the design parameter.

Figure 6 compares the target geometric profile with the initial guess profile, the first iteration profile, and the optimal profile as determined by Broyden's algorithm. The correct geometry was obtained in four iterations, which required five function evaluations (CFD solutions). Figure 7 shows typical variation of flow variables at the RP as evidenced by Mach number profiles. Figures 8 and 9 show the reduction of the objective function and the convergence history of the design parameter, t, versus iteration number, respectively. As evidenced by these figures, the Broyden's algorithm isolated the global minimum quite efficiently. The data from which Fig. 9 was produced indicates that the optimum was located within 1 percent in 2 iterations and was isolated within 0.1 of 1 percent in 4 iterations.

Airfoil optimization has been performed by several other researchers by prescribing a pressure distribution along the airfoil surface and solving a true inverse problem. As an interesting example of the versatility of the nonlinear least-squares approach, the previously described design problem was also solved by forming the least-squares objective function from the difference between the airfoil surface pressures for a given design point and a specified pressure distribution. The target pressure distribution was obtained as before by applying PARC2D to compute the inviscid flow field about this airfoil, subject to the previously described boundary conditions (Fig. 3). The airfoil surface pressure distribution was then used to form a nonlinear least-squares objective function, defined by

$$\underline{R}^T\underline{R} = \sum_{i=1}^{N} (P_{rp} - P)_i^2 \tag{13}$$

where P_{rp} denotes the desired airfoil surface pressure at one of the N RP locations, and P denotes the airfoil surface pressure for a given design point. Optimization of the airfoil in this manner produced results very similar to those obtained by defining a trailing edge reference plane. This is illustrated in Fig. 10 by the reduction in the objective function and in Fig. 11 by the convergence of the design parameter, t. For this formulation the optimum was located within 2 percent in 4 iterations and was isolated within 0.3 of 1 percent in 6 iterations.

3.2 VISCOUS FLOW ABOUT A PLANAR AIRFOIL

Formulating the aerodynamic design problem as a nonlinear least-squares minimization allows flexibility in selecting the type of CFD simulation as well as allowing application to complex designs. For example, inclusion of viscous effects does not necessitate any changes to the applied optimization algorithm. The difference in the overall optimization process occurs only in the CFD analysis step. In other words, a more elaborate CFD simulation provides the various function evaluations, but the optimization algorithm does not recognize that the origin of the function evaluation assumed a more complex physics model.

As a simple demonstration of a design problem in which viscous effects were included, the previously described NACA0012 airfoil was analyzed with function evaluations supplied by viscous, Navier-Stokes simulations. As for the inviscid flow over the airfoil, PARC2D was used to define the target RP properties by computing viscous flow about a NACA0012 airfoil, subject to the indicated boundary conditions (Fig. 12). The imposed boundary conditions were identical to those used for the inviscid airfoil example, except the airfoil surface was modeled as a no-slip, adiabatic wall rather than an inviscid, slip-wall boundary. A free-stream Reynolds number of 106, based upon chord length, was specified, which produced an attached laminar boundary layer (Fig. 13) when analyzed with PARC2D. In this example, the RP was extended three chord lengths into the domain from the airfoil trailing edge. The design parameter (airfoil thickness) was perturbed to 1/12 its original value as an initial guess to begin the optimization. Broyden's quasi-Newton algorithm was then applied to derive the optimal value of the parameter. Because of the similarity to the inviscid problem, no sensitivity study of the design variable was performed.

Figure 14 compares the target geometric profile with the initial guess profile, the first iteration profile, and the optimal profile as determined by Broyden's algorithm. The correct geometry was obtained in three iterations, which required five function evaluations (CFD solutions). Figures 15 and 16 show the reduction of the objective function and the convergence history of the design parameter, t, to the known optimum. Again, Broyden's algorithm isolated the global minimum very efficiently. The data from which Fig. 16 was produced indicates that the optimum was located within 1 percent in 2 iterations and was isolated within 0.1 of 1 percent in 3 iterations.

This viscous example was modified by choosing an initial guess for the design parameter that was double the correct value, producing a much thicker initial airfoil contour. This posed a more difficult optimization problem because the computed flow field about the initial guess airfoil was separated (Fig. 17), whereas the computed flow field about the target airfoil was attached for the prescribed boundary conditions (Fig. 13). The absence or presence of separated flow within the design space provided an abrupt change in the flow field for candidate designs

in very nearly a discontinuous fashion. To assess whether the optimization technique is robust enough to optimize designs for which flow separation may occur, this airfoil was analyzed with the RP deliberately placed within the region of separated flow. The RP was located at the trailing edge and extended from the airfoil surface to the edge of the computational domain. As with prior examples, PARC2D was used to provide function evaluations at the RP.

Convergence for this example was similar to earlier results, although somewhat slower, with the optimum design variable located within 1 percent in 5 iterations and to within 0.1 of 1 percent in 6 iterations requiring 7 function evaluations. Figure 18 illustrates the convergence to the target geometry by comparing the target geometric profile with the initial guess profile, the first iteration profile, and the optimal profile as determined by Broyden's algorithm. Figures 19 and 20 illustrate the reduction of the objective function and the convergence of the design parameter, t, to the known optimum, respectively. The prominent slope change in Fig. 19 coincides with the first candidate design for which minimal separated flow was present.

3.3 INVISCID PLANAR CONVERGENT/DIVERGENT NOZZLE FLOW

Optimization of multiple aerodynamic design parameters was illustrated by analyzing inviscid, planar, supersonic flow in a nozzle (Fig. 21). The design variables for this problem were inflow total pressure, inflow total temperature, and the nozzle wall contour defined as a three-parameter Bezier curve. The vectors used to define the Bezier curve were located axially at the inlet plane, the midpoint, and the exit plane as indicated in Fig. 21. The exit plane control vector was held constant during the optimization. The y coordinate of the other two vectors were allowed to vary as design parameters during the optimization (Fig. 21). In addition to these two geometric parameters, the nozzle inlet total temperature and the nozzle inlet total pressure were allowed to vary, yielding a total of four design parameters. Each parameter was nondimensionalized by an appropriate reference quantity. The Bezier parameters were normalized by the target nozzle inlet height, total pressure by the target total pressure, and total temperature by the target total temperature.

The simultaneous variation of inlet total conditions and nozzle wall contour is not necessarily representative of a typical nozzle design problem, but this example was constructed because simultaneous variation of free-jet total conditions and a variable geometry occurs with the supersonic forebody simulator design problem that motivated the present research. The target solution was defined by selecting the Bezier parameters to produce a nominal 2:1 area ratio nozzle and applying PARC2D to solve the Euler equations using 1,600 grid points to resolve the domain. To form an initial guess, the inflow height and the nozzle throat height were reduced so that the initial nozzle area ratio was approximately doubled and the nozzle throat was shifted forward. The initial guess inflow total temperature and total pressure values

were doubled. The disparity between the target design and the initial guess is illustrated by comparing the centerline Mach number profiles for the target design and for the initial guess (Fig. 22). As can be seen, the exit target Mach number was nominally 50 percent below the initial guess with a corresponding variation within the rest of the nozzle. Again, no special effort was made to produce a highly accurate simulation, although results agree well with one-dimensional theory (Fig. 23).

Broyden's quasi-Newton algorithm was again applied in this example. For the first iteration, the Jacobian was approximated by a one-sided finite difference of each of the N residuals, as illustrated in the following example for the partial derivative of the i^{th} residual with respect to the j^{th} parameter

$$\frac{\partial r_i}{\partial P_j} = \frac{r_i(P_1,\ldots,P_j + \Delta P_j,\ldots,P_M) - r_i(P_1,\ldots,P_j,\ldots,P_M)}{\Delta P_j} \tag{14}$$

As with the airfoil example, the partial derivative of the objective function with respect to each of the geometric design parameters was investigated by performing a sensitivity analysis based on comparing derivative accuracy versus the size of ΔP_j used in Eq. (14).

Figure 24 depicts the variation of the normalized objective function differences, as given by Eq. (14), with respect to one of the Bezier design parameters, P_1, versus the log of the parameter step size. As can be seen, this derivative is sensitive to step size, but attains a nearly constant value for step sizes between 0.0001 and 0.002. Between these limits, the partial derivative is constant within 0.5 percent. The inaccuracy observed for large step sizes reflects the nonlinearity of the problem and the inaccuracy introduced by neglecting higher order terms in the difference approximation. The inaccuracy for very small step sizes results from numerical errors in the function evaluations becoming of the same order as the true difference in functional value. From this data a step size of 0.001 was selected for the Bezier parameters. For an Euler simulation, the residuals vary linearly with total temperature and total pressure; thus, these parameter step sizes are not as critical in this example. A nondimensional step size of 0.001 was selected for the fluid dynamic parameters to be consistent with the geometric parameters.

The optimization algorithm converged to the global minimum in four iterations, which required nine function evaluations. Typical convergence of the reference plane properties is illustrated in Fig. 25, which shows reference plane Mach number profiles for the target solution, the initial guess, the first iteration, and the optimum. The reduction in the objective function is illustrated in Fig. 26. During the optimization, inflow total conditions converged to within 1 percent of the correct value in 1 iteration. This is because, for this example, RP pressures and temperatures scale linearly with the specified total conditions. Thus, the residuals vary linearly with these parameters, and rapid convergence was expected since a Gauss-Newton-

type algorithm was applied. In fact, for an optimization problem in which the residuals are linear in all of the parameters, it is well known that a Gauss-Newton algorithm converges to the exact solution in one iteration. The geometric parameters converged more slowly but still at an acceptable rate. The convergence of the full geometry defined by the individual parameters is illustrated in Fig. 27, which shows the iterative variation of the nozzle wall contour. The convergence of the individual design parameters to the correct solution is illustrated by Figs. 28 through 31.

3.4 INVISCID THREE-DIMENSIONAL NOZZLE FLOW

A 3-D rectangular nozzle (Fig. 32) was used to demonstrate that the nonlinear least-squares optimization method is applicable in three dimensions. The nozzle geometry and interior grid were defined by 3-D Bezier polynomials, Eq. (9). Four control points were specified at each of five axial planes so that each axial cross section was rectangular. The entire volume was then defined using the coordinate vectors of these 20 control points to define the Bezier polynomials. Two design parameters were defined as coefficients, P_1 and P_2, that controlled the length and width of the rectangular cross section at the midplane (Fig. 32). The target geometry corresponded to values of unity for each parameter, which produced a nozzle with a nominal exit-to-throat area ratio of 2.5. Total conditions were specified at the nozzle inlet. A static pressure below second critical was selected at the nozzle exit. This allowed fully supersonic flow to develop in the divergent portion of the nozzle. These geometry and boundary conditions produced a flow field with a nominal exit Mach number of 2.5 when analyzed with the Euler version of the PARC3D code.

For an initial guess, the design parameters P_1 and P_2 were set equal to 2.0 and 2.5, respectively. This produced a nozzle with a nominal exit-to-throat area ratio of 64. A PARC3D analysis of this geometry subject to the described boundary conditions produced a flow field with a nominal exit Mach number of 5.8 using 23,000 grid points in the simulation. Unlike the target nozzle, which was square at each axial cross section, the initial guess nozzle had a square cross section at the inflow plane, which transitioned to a rectangular cross section at the midplane, and then transitioned again to a square at the exit plane. The large differences in exit flow conditions for the initial guess nozzle compared to the target nozzle were selected to illustrate that the initial guess flow field does not necessarily need to closely resemble the desired optimum to obtain acceptable results. The differences in the flow fields for the target nozzle and the initial guess nozzle geometries are illustrated by comparing the centerline Mach number profiles for the two designs (Fig. 33). Also presented are the distributions for the first iteration and for the computed optimum.

A sensitivity analysis was performed on design parameter P_1 that indicated that parameter step sizes ranging from 0.0001 to 0.01 produce nearly the same objective function derivative

(Fig. 34). The variation in Fig. 34 reflects the sensitivity to parameter step size attributable to nonlinear effects and numerical error inherent in the objective function evaluations. A value of 0.001 was selected for the design variable step size in this example. Application of Broyden's quasi-Newton algorithm did not converge to the correct optimum for this test case. It is suspected that the Jacobian computation was not accurate enough for reliable application of quasi-Newton algorithm. When the Gauss-Newton algorithm was applied, the RP properties converged in 6 iterations requiring 18 function evaluations. Figures 35 and 36 provide an example of the RP convergence by comparing y and z centerline Mach number profiles at the RP for the target solution, the initial guess, the first iteration, and the computed optimum. The achieved reduction in objective function and the design parameter convergence is depicted in Figures 37 and 38, respectively, which illustrate that the global minimum of the objective function was isolated. Convergence is further demonstrated by comparing the wall contours for constant y planes (Fig. 39) and constant z planes (Fig. 40).

3.5 INVISCID SUPERSONIC FLOW ABOUT A PLANAR FOREBODY SIMULATOR

A 3-D analog to the motivating design problem was constructed and is shown in Fig. 41. The configuration shown was used to define the target flow variables at the indicated reference plane. Thirteen thousand grid points were used to resolve the domain, which was analyzed inviscidly by the application of PARC2D in the Euler mode. In this example, the Mach number at the inflow plane was treated as a design variable to represent the variable free-jet Mach number that would be encountered in the motivating design problem. The forebody simulator geometry was defined as a Bezier curve with four variable parameters. The geometric design variables were normalized by the forebody simulator height, and the Mach number design variable was normalized by the target Mach number to make each design variable of the same order. The RP was located one inlet height in front of the inlet entrance.

The target design was a relatively blunt forebody with an incoming Mach number of 3.0 (Fig. 41). The reference plane was located downstream of the detached shock emanating from the leading edge of the forebody. Also within the flow field, weak shocks reflect from the cell wall boundary and from the nozzle walls. The simulation was run with an exit pressure low enough to maintain fully supersonic flow across the computational exit plane. The five design parameters shown in Fig. 41 were then perturbed to initialize the optimization. For the initial guesses, the Mach number was increased by 50 percent, and the geometric parameters were reduced by 10 to 70 percent to intentionally provide a poor initial guess.

The disparity between the target design and the initial guess configuration is illustrated by comparison of the respective Mach number contours (Fig. 42 and 43). As can be seen, the shock structures in front of the reference plane are very different, leading to large discrepancies in RP flow variables. The forebody shock passes very close to the RP in the initial guess configuration, which further complicates the optimization task.

The RP objective function was minimized by the application of the Gauss-Newton algorithm. Analysis of the objective function gradients indicated that the minimum derivative variation was about 2 percent (Fig. 44) for nondimensional, geometric variable step sizes between 0.02 and 0.05. These derivatives were not accurate enough for successful application of the quasi-Newton algorithm. However, when the Gauss-Newton algorithm was applied, convergence was obtained in five iterations requiring 31 function evaluations. The maximum Mach number deviation, at the RP, was less than 1 percent after only two optimization steps requiring 13 function evaluations, which for many applications, may be adequate. A comparison of the reference plane Mach number profiles for the initial guess, the target solution, and the final converged solution is made in Fig. 45, which shows excellent agreement between the target and final solutions. Figure 46 plots the objective function versus design iteration number illustrating that the global minimum of the objective function was isolated. The convergence history for each of the five design parameters is illustrated in Fig. 47.

3.6 INVISCID SUPERSONIC FLOW ABOUT A REDUCED LENGTH FOREBODY SIMULATOR

The motivating design problem requires that RP properties be matched within design tolerance while significantly shortening the actual aircraft forebody. An example emulating this type of optimization problem was constructed by seeking a forebody half the length of the described target forebody as depicted in Fig. 41 and retain the RP target values defined in Section 3.5. This length restriction excluded an exact match of RP variables from the optimization design space. Each candidate design was analyzed as a full test cell configuration without using a plane of symmetry as with the target configuration. Each design was analyzed inviscidly by the application of the blocked version of PARC2D in the Euler mode using 26,000 grid points to resolve the domain in each CFD simulation.

The optimization problem was constructed using four design variables. The inflow plane Mach number (normalized by M = 3.0 as a reference Mach number) was used as a fluid dynamic design variable. The forebody simulator geometry was again defined as a Bezier curve with the vertical component of three of the Bezier control vectors used as design variables. These geometric design variables were normalized by a reference length equal to the height of the target forebody. As with the full-length forebody design, the Gauss-Newton algorithm was applied. In three iterations, requiring 16 function evaluations, the deviation from normalized RP objective function components of total pressure and axial Mach number was as indicated in Figs. 48 and 49. In these figures, each RP component was normalized by the corresponding target value to facilitate comparison of the various design iterations. The target values for the vertical Mach number component were very near zero; thus, comparison of the actual residual components is most meaningful and is presented in Fig. 50. The total temperature component of the objective function is not presented since total temperature remains constant, within numerical accuracy, for this inviscid computation.

As seen from Figs. 48 through 50, each component of the objective function was reduced from its initial value. The convergence and rate of reduction of the total objective function is further illustrated in Fig. 51. Further iterations failed to yield any appreciable reduction in the objective function. Additionally, the contribution from the total temperature components to the objective function sum became of the same order as the total pressure and Mach number components. This indicated that further reduction in the objective function was unlikely, since for the Euler simulations, any mismatch in total temperature could be attributed to numerical error. The comparison of the RP Mach number for various iterations, as shown in prior examples, is presented in Fig. 52. The variation of the geometric contour is illustrated in Fig. 53. In this two-dimensional example, the Gauss-Newton algorithm was able to substantially reduce the deviation of RP fluid dynamic parameters from the prescribed distributions leading to a substantially improved design. The number of required function evaluations is also within practical limits using current technology.

4.0 USAGE CONCEPTS

The computer program that was used to generate the previous results is available for application at the AEDC. Although it is still a developmental code, it is relatively easy to apply. This section is not intended to serve as a complete user's guide for the developmental code, but will serve to briefly describe information required to apply the design optimization code in its present form.

Input variables required by the code are supplied through a namelist format. However, before defining the necessary input variables, an overall description of the design process is helpful. Examination of Fig. 2 reveals four key steps in the design optimization process, (1) definition of design variables, (2) analysis of the candidate design, (3) measure of the design quality, and (4) adjustment of the design variables.

Design optimization methods are intended to assist the engineer in developing a quality design. They are not intended to eliminate the need for good engineering judgment. Defining the design variables and measuring the design quality are two areas where a thorough understanding of the design requirements and a recognition of the important design parameters is essential to developing a quality design. Within this research, a least-squares norm at the IRP was used as an objective function to measure the design quality. This objective function was assumed to be a function of the selected design variables. If the IRP objective function is not responsive to variation of the selected design variables, then the problem is not well defined. It must also be remembered that design variable specification defines the allowable design space that will be searched for the optimal design. If the defined design space is too restrictive, the resulting design may be unsatisfactory even though the optimal value, within the allowable design space, was properly located. This is one of the reasons that the Bezier

surfaces were selected for geometric parameterization. They exhibit the desirable features of providing a wide range of geometric flexibility for a relatively small number of design variables. An increase in the number of design variables directly increases the number of function evaluations (CFD simulations) required to attain an optimum.

As with any CFD simulation, all results should be carefully analyzed. For the coupled optimization method, multiple CFD simulations are combined to determine design space gradients that iteratively leads to an optimized design. If the results of the simulations are not consistent and reliable, then poor results are to be expected (garbage-in yields garbage-out). Some items to pay particular attention to include (1) large variations in grid quality between simulations, (2) temporal variations attributable to inherent unsteadiness or poor convergence, and (3) generally poor results near the IRP.

For an N-dimensional design problem, a CFD simulation is required for the base design and N perturbations to the base design. The perturbation value is specified by the user and should be consistent with the design variable. Typically, this value is determined by examining the design space as described in Section 3 of this report. The optimization code is executed as a postprocessor after each CFD simulation to evaluate the objective function and to compute the value of each design variable to be used for the next function evaluation. One initialization run is required to establish target IRP values. In this manner, the optimization code guides the engineer to the optimal design.

4.1 FILE USAGE

The job control file must fetch necessary input files, compile, load, and execute the source code and dispose generated output files. The source code requires four input files as follows:

1. **Unit # 2** — a PARC format restart file corresponding to the current set of design variables.

2. **Unit # 3** — the optimization code restart file, which contains IRP flow variables and IRP grid coordinates for all prior design iterations.

3. **Unit # 5** — a namelist input file that contains code variable definitions to control program execution.

4. **Unit # 9** — a design variable history file that is used to monitor the iterative behavior of the design variables and convergence toward the optimal design.

Two output files are created containing

1. **Unit # 7** — the updated optimization code restart file.

2. **Unit # 10** — the updated optimization code design variable history file.

Coupling the optimization code to an analysis code other than PARC would necessitate minor changes in the input subroutine.

4.2 NONDIMENSIONALIZATION

Since diverse flow properties are used to comprise the IRP residuals, each residual component is normalized by a user-selected reference value, as noted in Section 2.3.2. A general recommendation is to make each residual term of order one, in which case each component of the residual will be driven to zero at approximately the same rate. However, there may be instances where the user wishes to bias the solution by weighting one set of residuals more heavily than other residuals. This can be accomplished by choosing an appropriate set of reference properties.

4.3 NAMELIST CONTROL

All user inputs to the design code are provided from Unit # 5 through the namelist titled "Control." These inputs are used to define (1) PARC nondimensionalization variables, (2) design code nondimensionalization variables, (3) IRP target value definition, (4) variable geometry indices, and (5) optimization code operation. Some variables contained within this namelist are strictly for code development and diagnostic use. Description of variables needed to execute the design optimization code are

DTH	Real vector specifying the perturbation value for each design variable during derivative computations
IBACKUP	Development and diagnostic use
IC1	Integer vector identifying the set of candidate designs to use within the current optimization step
FMACH	The reference Mach number used to normalize the directional Mach number residual components
GAMMA	PARC code specific heat ratio

IBPATH	Integer vector specifying the set of candidate designs needed to form quasi-Newton Jacobian algorithm (Broyden's update formula)
JEGEO	Beginning j-index for the variable design geometry. Used only for postprocessing of results.
JIRP	IRP j-index
JSGEO	Variable design geometry ending j-index. Used only for postprocessing of results.
KEGEO	Variable design geometry beginning k-index. Used only for postprocessing of results.
KSGEO	Variable design geometry ending k-index. Used only for postprocessing of results.
KEIRP	IRP ending k-index
KSIRP	IRP starting k-index
KSKIP	Skip factor to specify the frequency with which a full Gauss-Newton optimization step is performed. KSKIP = 1 implies all steps will be Gauss-Newton, KSKIP = 5 implies every fifth step is Gauss-Newton with all other steps quasi-Newton, etc.
LEGEO	Variable design geometry beginning l-index. Used only for postprocessing of results.
LSGEO	Variable design geometry ending l-index. Used only for postprocessing of results.
LEIRP	IRP ending l-index
LSIRP	IRP starting l-index
NCASES	The cumulative number of candidate designs
NCYCBACK	Development and diagnostic use

NBROYSTP The number of designs used to execute the Broyden update formula

NSTART Initialization parameter. If NSTART = 0 the code performs a first pass initialization to define IRP values

PREF PARC code reference pressure

PTNORMAL The reference pressure used to normalize the total pressure residual components

TREF PARC code reference temperature

TTNORMAL The reference temperature used to normalize the total temperature residual components

5.0 SUMMARY AND CONCLUSIONS

A direct aerodynamic design optimization technique that couples an existing Euler/Navier-Stokes solver with efficient nonlinear least-squares minimization algorithms has been developed and demonstrated by successfully applying the technique to representative aerodynamic design problems. This demonstrated that design space gradients, required by the Gauss-Newton-based optimization algorithms, could be reliably formed from Euler/Navier-Stokes CFD simulations. In fact, for two examples presented, a quasi-Newton algorithm was successfully applied to determine the optimal design variables. The examples were deliberately started from poor initial designs to assess the capability of the design technique to converge from poor initial conditions. Although this does not yet achieve the desired 3-D forebody simulator design capability, it does represent significant progress toward satisfaction of that goal.

To date, this research has evaluated the feasibility of coupling nonlinear optimization methods with CFD. Existing Gauss-Newton and quasi-Newton optimization algorithms were employed with minimal modifications with good results obtained for several representative aerodynamic design problems. The quasi-Newton algorithm was not successful for the more aerodynamically complex examples, but was significantly more efficient when applicable. This suggests that alternating between the two algorithms may produce a more efficient optimization strategy if reliable switching criteria can be determined. Because of the complexity of the motivating application, the optimization algorithms were coupled with an Euler/Navier-Stokes CFD code, which makes the function evaluations computationally expensive. However, the same method could be coupled with a less complex CFD technique for design problems in which an Euler or Navier-Stokes simulation is not required.

The approach presented provides the designer with a potentially powerful tool to assist in many designs for which a measure of design quality (objective function) can be adequately defined. Because of the flexibility afforded by the current CFD codes, this technique can be applied to virtually any steady-state aerodynamic optimization problem for which the selected CFD code is capable of providing a reliable aerodynamic analysis. The design method is reliable in the sense that improvements to the initial design are achieved, and it is efficient in terms of minimizing the number of function evaluations required to determine the optimal design variables. For complex 2-D aerodynamic designs, the method requires on the order of 10 to 50 function evaluations, depending upon the quality of the initial design, number of optimization parameters, and RP simulation tolerances. This number of function evaluations is feasible with access to modern supercomputers and use of appropriate CFD codes that efficiently yield the desired flow physics. As demonstrated by one simple example, the design method is applicable in three dimensions. However, the efficiency of the optimization process must be enhanced before this technology can be considered a practical 3-D design tool.

6.0 RECOMMENDATIONS

Achieving the "generation 6" forebody simulator design capability, proposed by the ASD/AEDC ASTF free-jet development technical steering committee, requires continued development of aerodynamic design optimization techniques. Computational fluid dynamics is certainly not a mature science and the use of CFD within a design optimization framework is in its infancy. If continued development of a "generation 6" design capability is deemed a priority item at the AEDC, then the following topics need to be investigated.

1. Investigate the application of design optimization via control theory as proposed by Jameson (Ref. 18).

2. Investigate the application of genetic algorithms (Ref. 19) to minimize the number of required CFD simulations.

3. Improve the present direct optimization method by combining the efficiency characteristics of the quasi-Newton algorithm with the reliability characteristics of the Gauss-Newton algorithm.

4. Develop a method of selecting the appropriate design variable step sizes that is more efficient than the standard sensitivity study.

5. Develop a technique that relaxes the requirement that each CFD simulation must be fully convergent.

6. Reduce computational costs by using lower order CFD analysis techniques (MOC, PNS, etc.) in preliminary design phases.

7. Reduce computational costs by improving the efficiency of the CFD analysis code.

8. Reduce the labor required to perform each CFD simulation.

Items 1 and 2 represent research in areas with tremendous potential. Both of these techniques have the potential to not only reduce the computational effort required to optimize a given design, but they could also extend the allowable design space without significant penalty. However, neither optimization method has been investigated or applied extensively to realistic design problems. Items 3 through 5 are ideas to improve the efficiency of the subject direct optimization method. Item 6 is a suggested engineering approach to reduce computational costs and total design time within the existing optimization framework. Items 7 and 8 address the CFD analysis portion of the design process, which is where the preponderance of computational resources and manpower is expended. Again, CFD is not a mature science and we must continue to explore more efficient and more accurate means of analysis in addition to ongoing efforts to extend the application of CFD to more geometrically and aerodynamically complex configurations.

REFERENCES

1. Beale, D. K. and Collier, M. S. "Validation of a Free-jet Technique for Evaluating Inlet-Engine Compatibility." AIAA Paper 89-2325, AIAA/ASME/SAE/ASEE 25th Joint Propulsion Conference, Monterey, California, July 1989.

2. Huddleston, D. H. "Aerodynamic Design Optimization Using Computational Fluid Dynamics." PhD Dissertation, University of Tennessee, Knoxville, Tennessee, December 1989.

3. Varner, M. O. "Application of Optimization Principles to Flexible Wall Nozzle Design — A Case Study." AIAA Paper 86-0775, AIAA 14th Aerodynamic Testing Conference, West Palm Beach, Florida, March 1986.

4. Huddleston, D. H. and Mastin, C. W. "Optimization Methods Applied to Aerodynamic Design Problems in Computational Fluid Dynamics." 7th International Conference on Finite Element Methods in Flow Problems, Huntsville, Alabama, April 1989.

5. Huddleston, D. H. and Mastin, C. W. "Optimization of Aerodynamic Designs Using Computational Fluid Dynamics." AGARD Specialists' Meeting on Computational Methods for Aerodynamic Design (Inverse) and Optimization, Loen, Norway, May 1989.

6. Cooper, G. K. and Sirbaugh, J. R. "The PARC Distinction: A Practical Flow Simulator." AIAA Paper 90-2002, AIAA/ASME/SAE/ASEE 26th Joint Propulsion Conference, Orlando, Florida, July 1990.

7. Phares, W. J. et al. "Application of Computational Fluid Dynamics to Test Facility and Experimental Design." AIAA Paper 86-1733, AIAA/ASME/SAE/ASEE 22nd Joint Propulsion Conference, Huntsville, Alabama, July 1986.

8. Huddleston, D. H., Cooper, G. K., and Phares, W. J. "A Computational Fluid Dynamics Evaluation of Test Cell Recirculation Effects on High-Bypass Turbofan Engine Surface Pressure Distributions." AIAA Paper 86-1384, AIAA/ASME/SAE/ASEE 22nd Joint Propulsion Conference, Huntsville, Alabama, July 1986.

9. Cooper, G. K. and Jordon J. "Analysis Tool for Application to Ground Testing of Highly Underexpanded Nozzles." AIAA Paper 87-2015, AIAA/ASME/SAE/ASEE 23rd Joint Propulsion Conference, San Diego, California, July 1987.

10. Cooper, G. K. and Phares, W. J. "CFD Applications in an Aerospace Engine Test Facility." AIAA Paper 90-2003, AIAA/ASME/SAE/ASEE 26th Joint Propulsion Conference, Orlando, Florida, July 1990.

11. Soni, B. K. "Two- and Three-Dimensional Grid Generation for Internal Flow Applications of Computational Fluid Dynamics." AIAA Paper 85-1526, AIAA 7th Computational Fluid Dynamics Conference, Cincinnati, Ohio, 1985.

12. Scales, L. E. *Introduction to Non-Linear Optimization*. Springer-Verlag, New York, 1985.

13. Hartley, H. O. "The Modified Gauss-Newton Method for the Fitting of Nonlinear Regression Functions by Least Squares." *Technometrics*, Vol. 3, May 1961, pp. 269-280.

14. Broyden, C. G. "A Class of Methods for Solving Nonlinear Simultaneous Equations." *Mathematics of Computation*, Vol. 19, 1965, pp. 577-593.

15. Faux, I. D. and Pratt, M. J. *Computational Geometry for Design and Manufacture*. Ellis Horwood Limited, Chichester, West Sussex, England, 1985, pp. 132-134, 218, 293.

16. Madabhushi, R. K., Levy, R., and Pincus, S. M. "Design of Optimum Ducts Using an Efficient 3-D Viscous Computational Flow Analysis." *Proceedings of the Second International Conference on Inverse Design Concepts and Optimization in Engineering Sciences ICIDES-II*, October 1987, pp. 147-166.

17. Jameson, A. and Mavriplis, D. "Finite Volume Solution of the Two-Dimensional Euler Equations on a Regular Triangular Mesh." *AIAA Journal*, Vol. 24, No. 4, April 1986, pp. 611-618.

18. Jameson, A. "Airfoil Design Via Control Theory." AGARD Specialists' Meeting on Computational Methods for Aerodynamic Design (Inverse) and Optimization, Loen, Norway, May 1989.

19. Goldberg, M. "Engineering Optimization via Genetic Algorithm." *Proceedings of the 9th Conference of Electronic Computation*, February 1986, pp. 471-482.

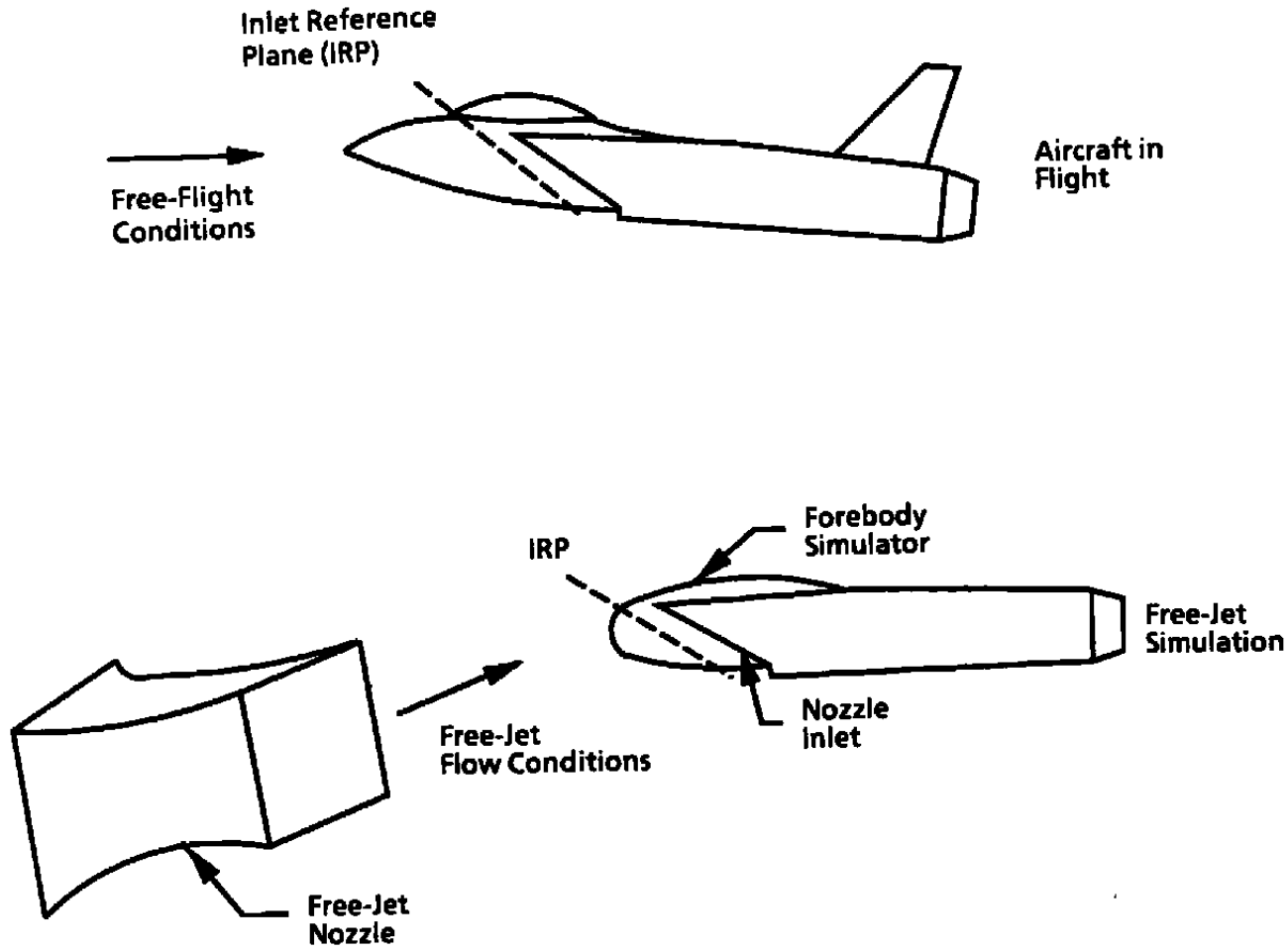

Figure 1. Generic free-jet engine/inlet compatibility test configuration.

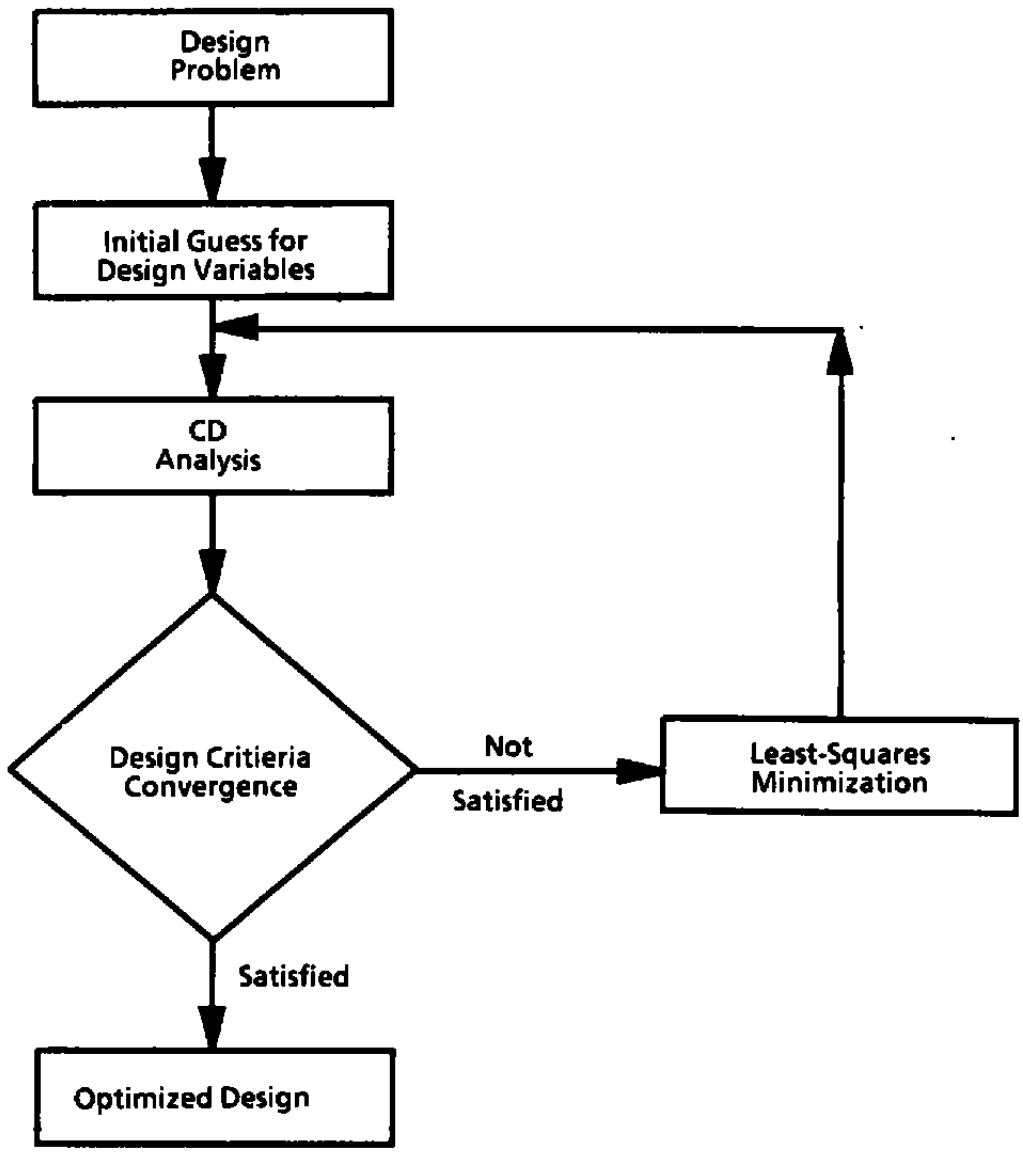

Figure 2. Design optimization strategy.

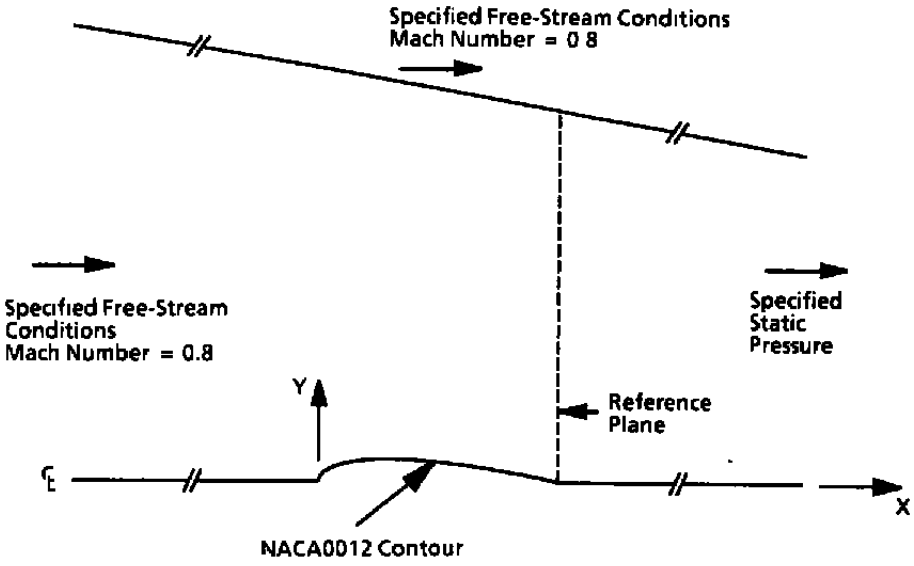

Figure 3. Inviscid airfoil optimization.

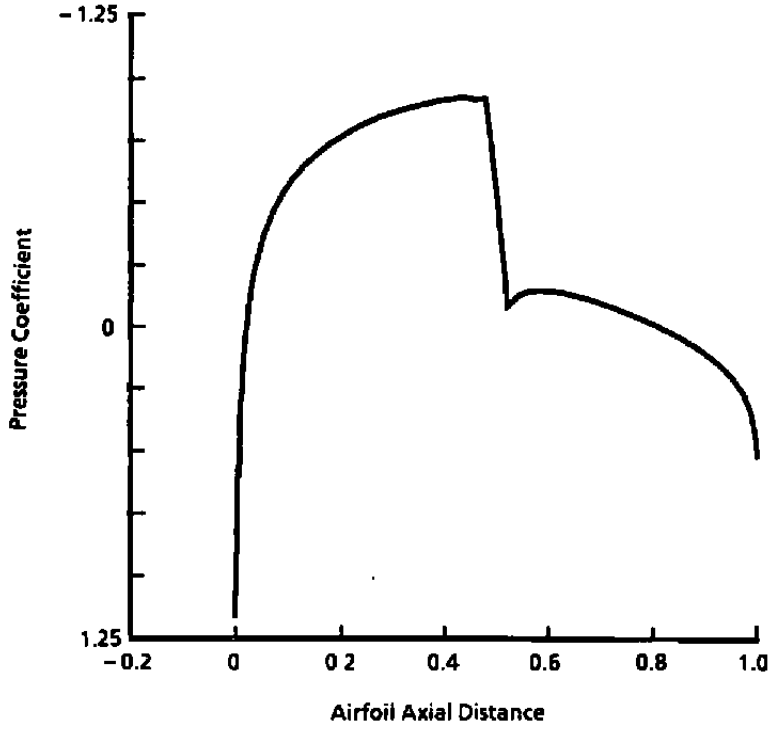

Figure 4. Inviscid airfoil surface pressure distribution.

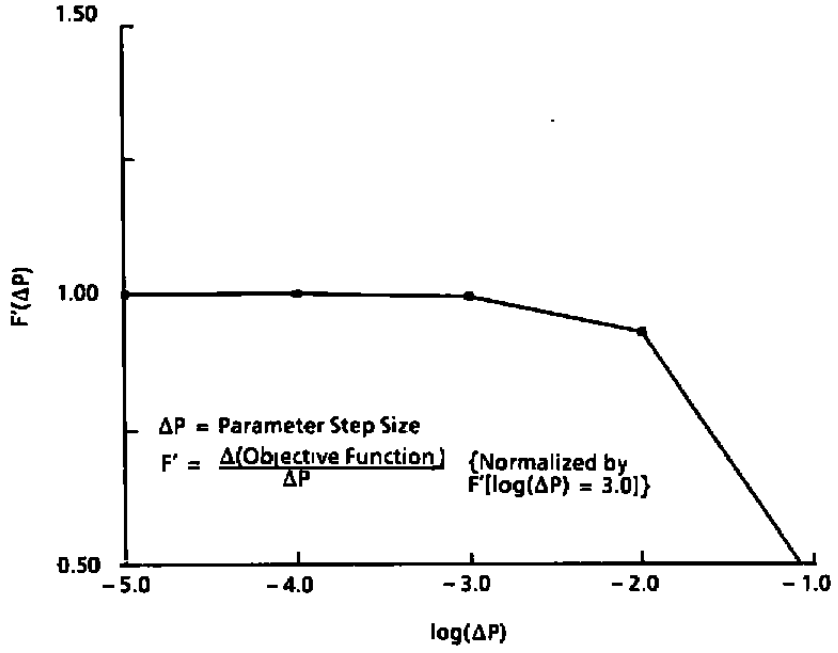

Figure 5. Inviscid airfoil derivative sensitivity.

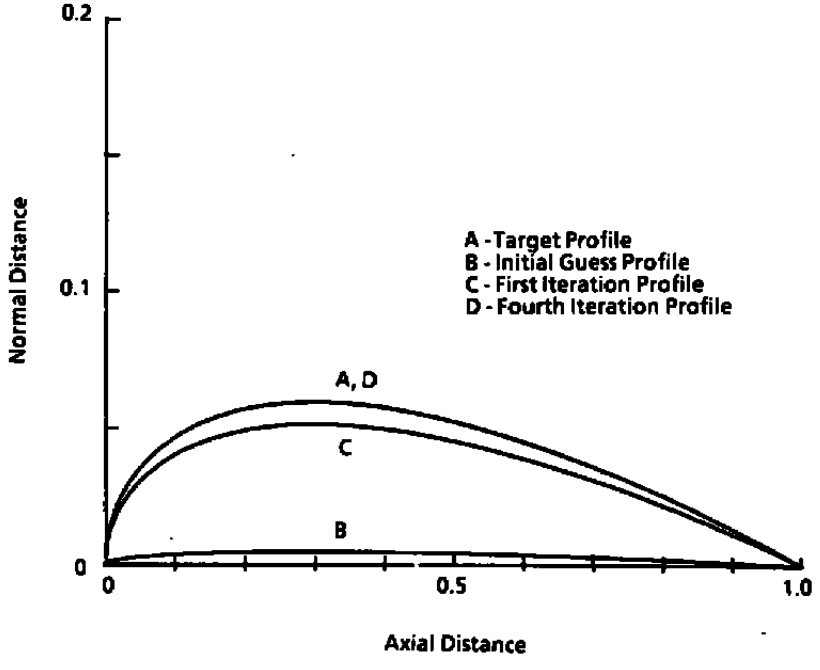

Figure 6. Inviscid airfoil contour variation.

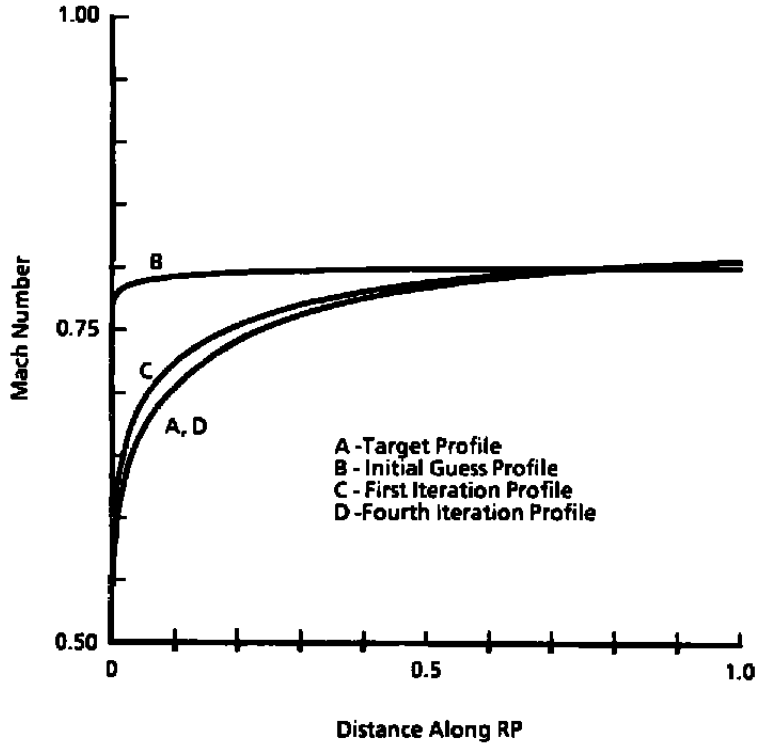

Figure 7. Inviscid airfoil reference plane Mach number profiles.

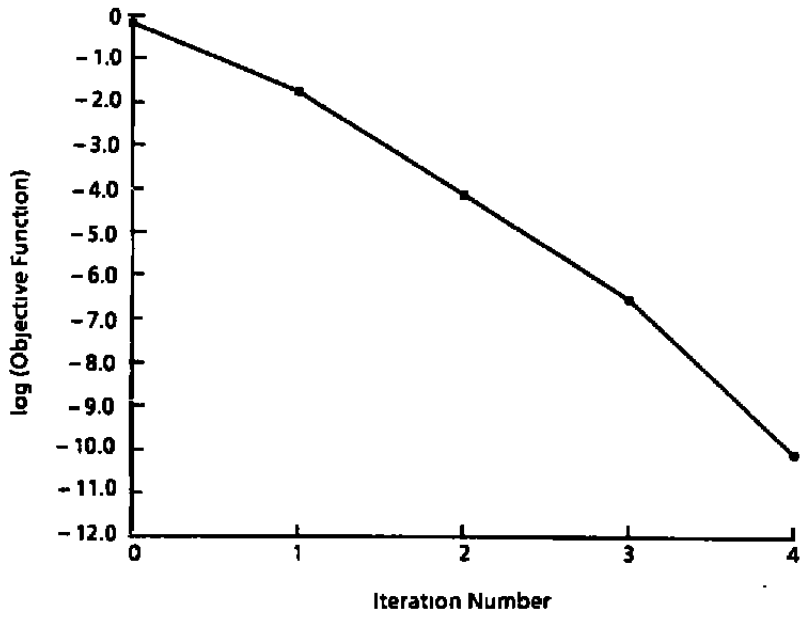

Figure 8. Inviscid airfoil objective function reduction.

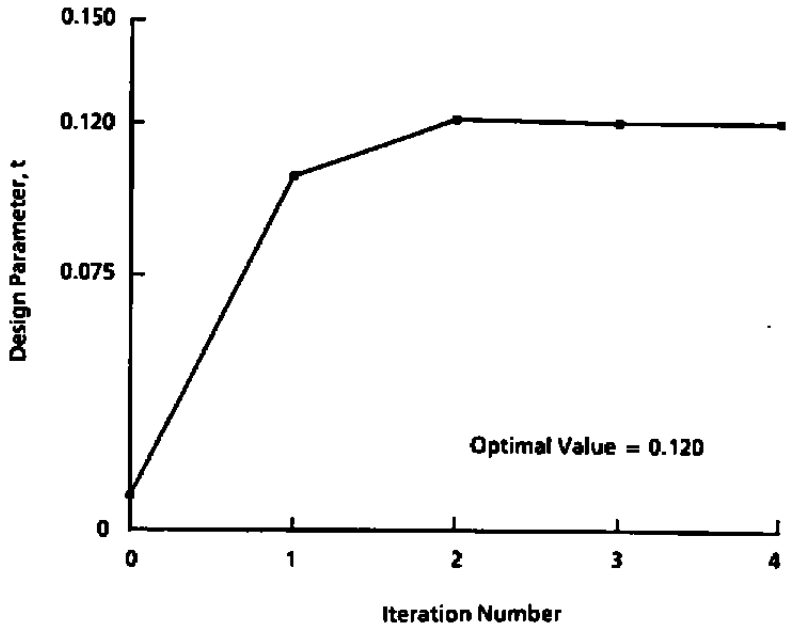

Figure 9. Inviscid airfoil design parameter convergence.

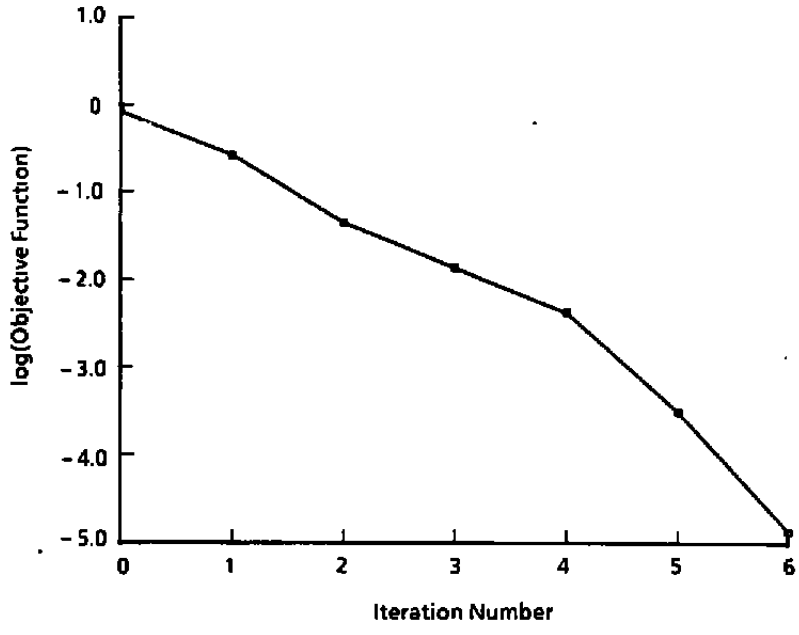

Figure 10. Inviscid airfoil objective function reduction for specified surface pressure distribution.

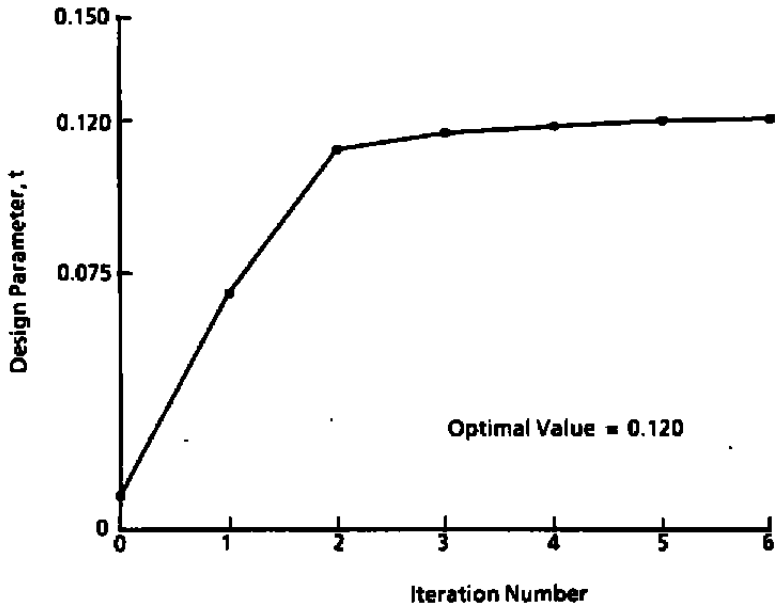

Figure 11. Inviscid airfoil design parameter convergence for specified surface pressure distribution.

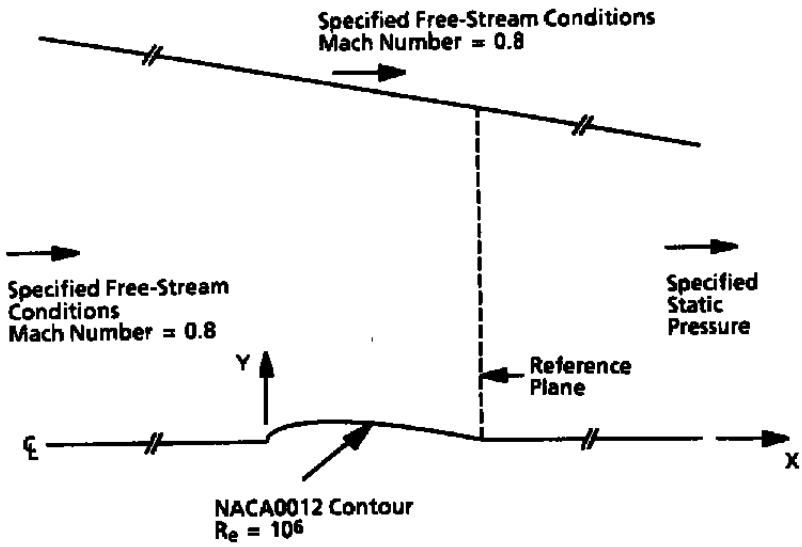

Figure 12. Viscous airfoil optimization.

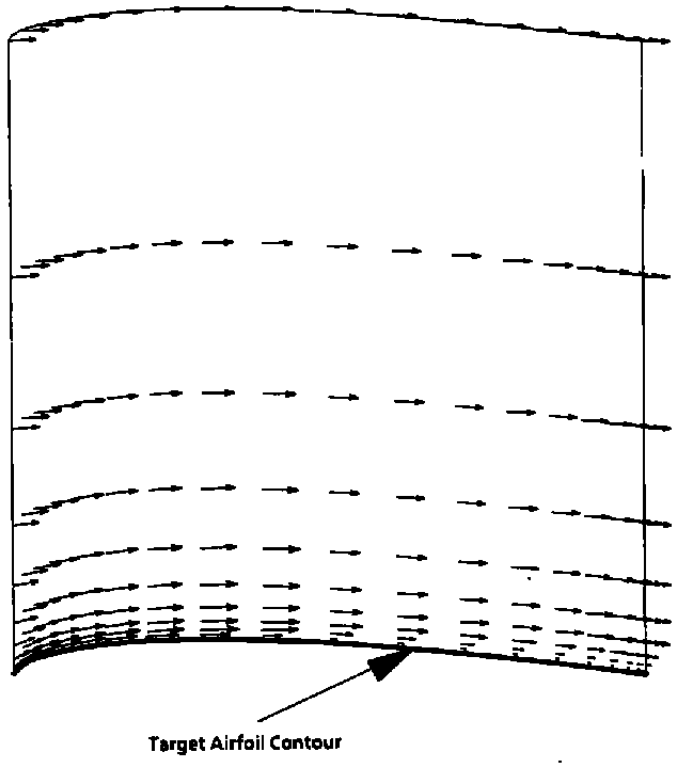

Figure 13. Viscous airfoil target velocity field.

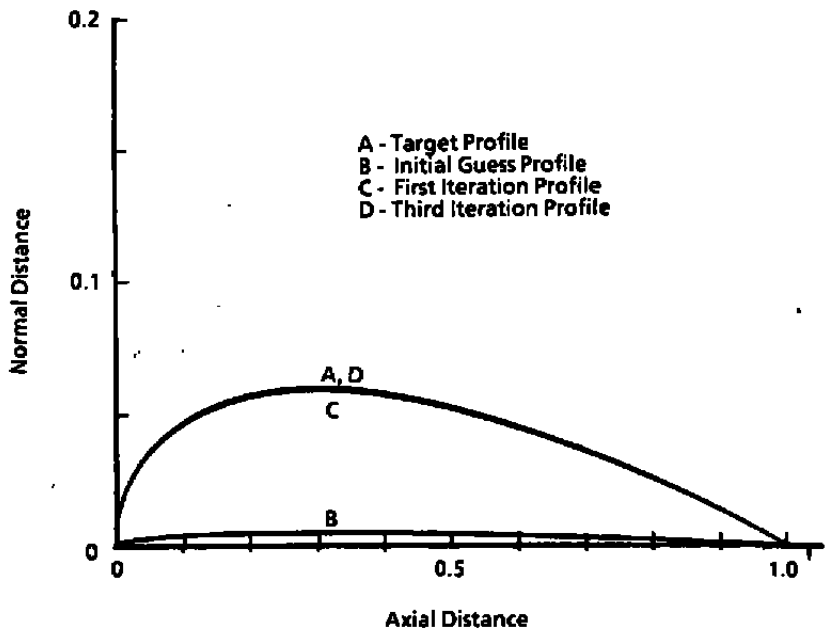

Figure 14. Viscous airfoil contour variation.

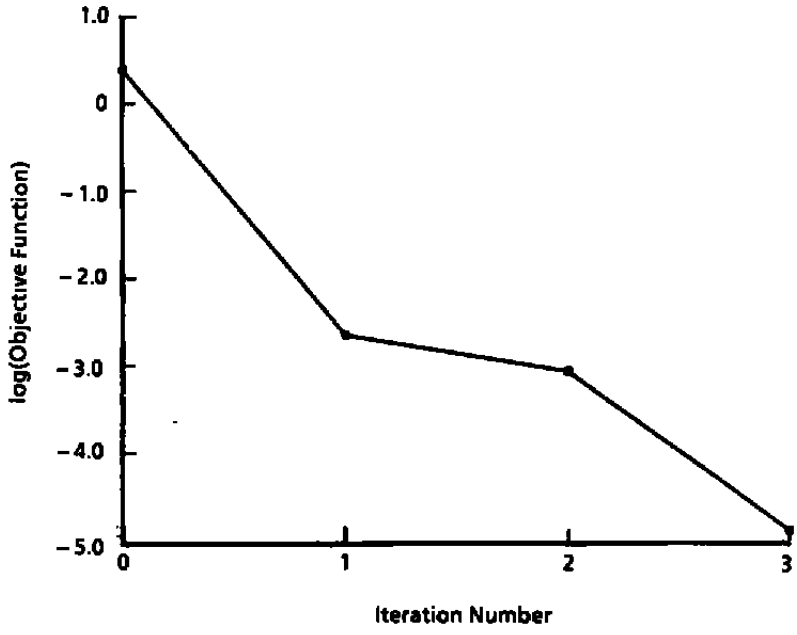

Figure 15. Viscous airfoil objective function reduction.

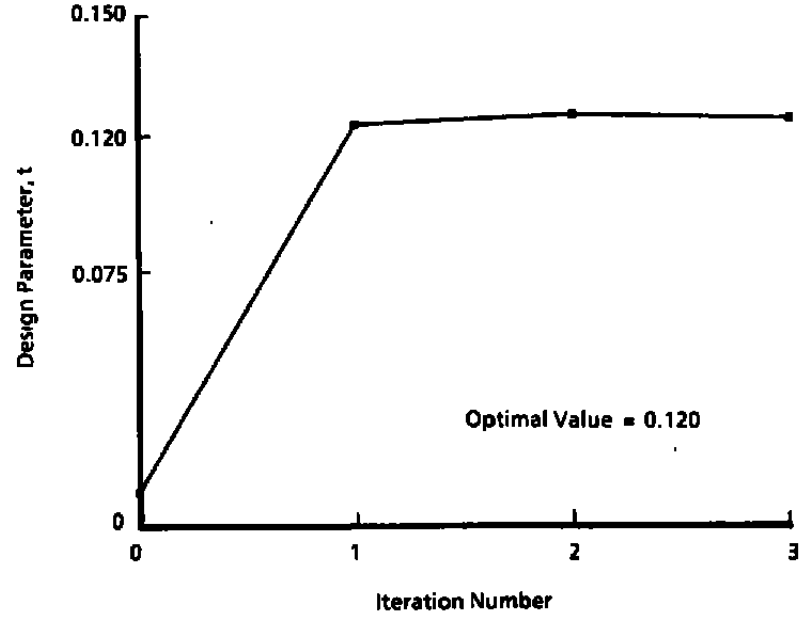

Figure 16. Viscous airfoil design parameter convergence.

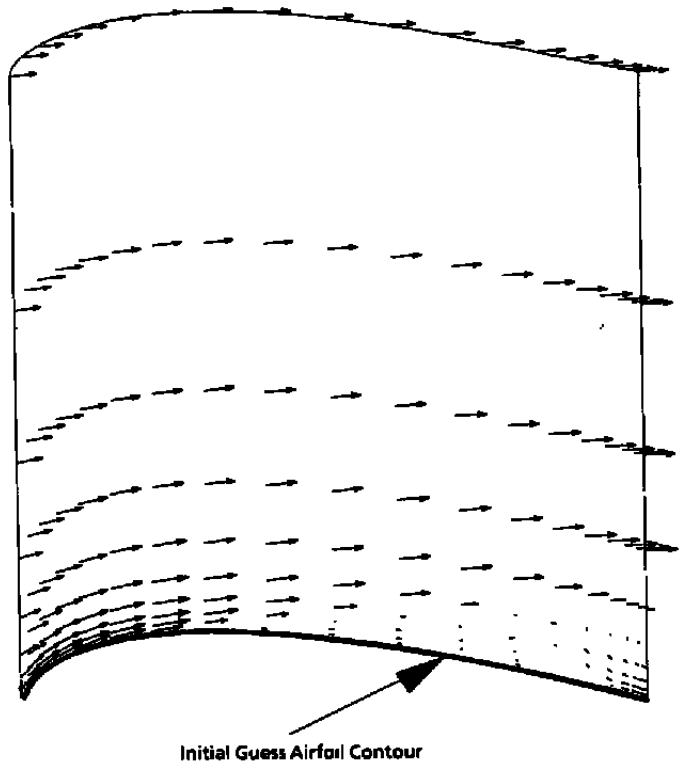

Figure 17. Separated viscous airfoil contour variation.

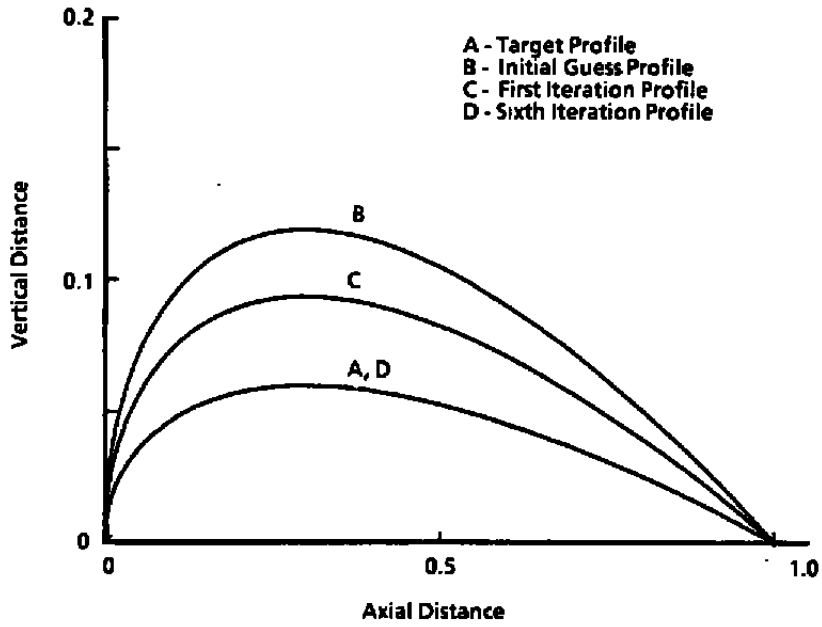

Figure 18. Separated viscous airfoil initial guess velocity field.

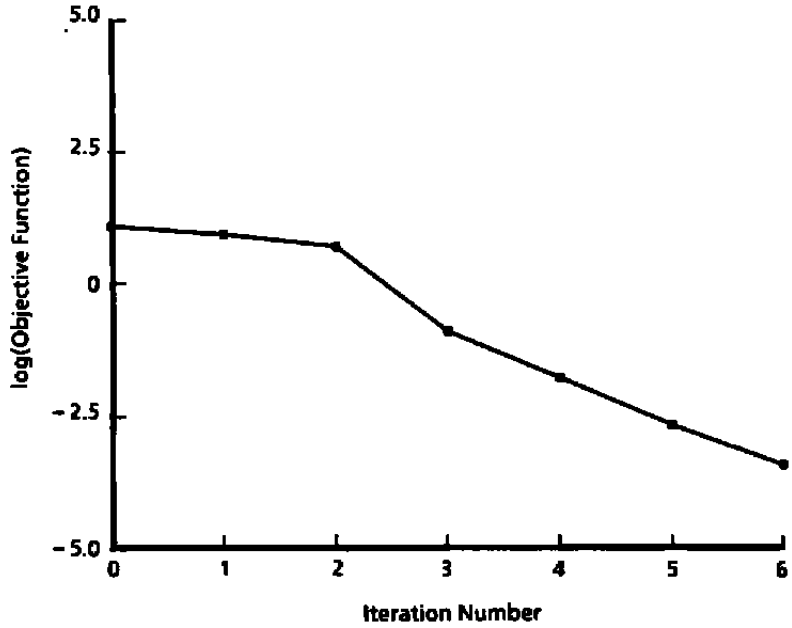

Figure 19. Separated viscous airfoil objective function reduction.

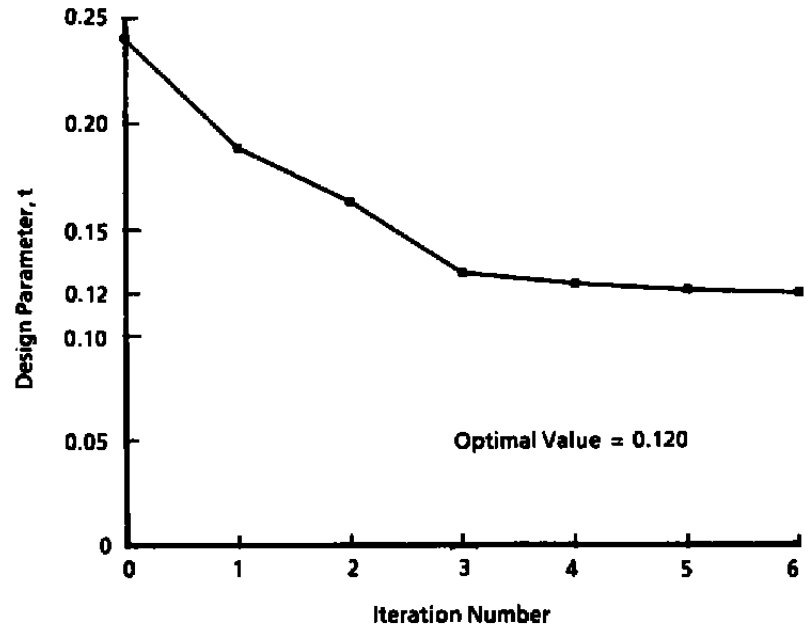

Figure 20. Separated viscous airfoil design parameter convergence.

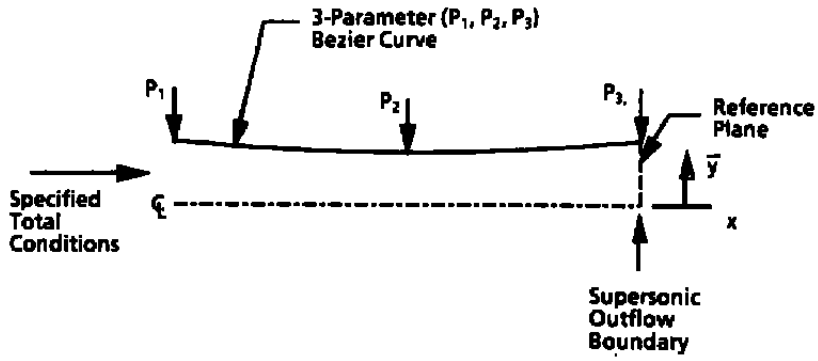

Figure 21. Planar convergent/divergent nozzle optimization.

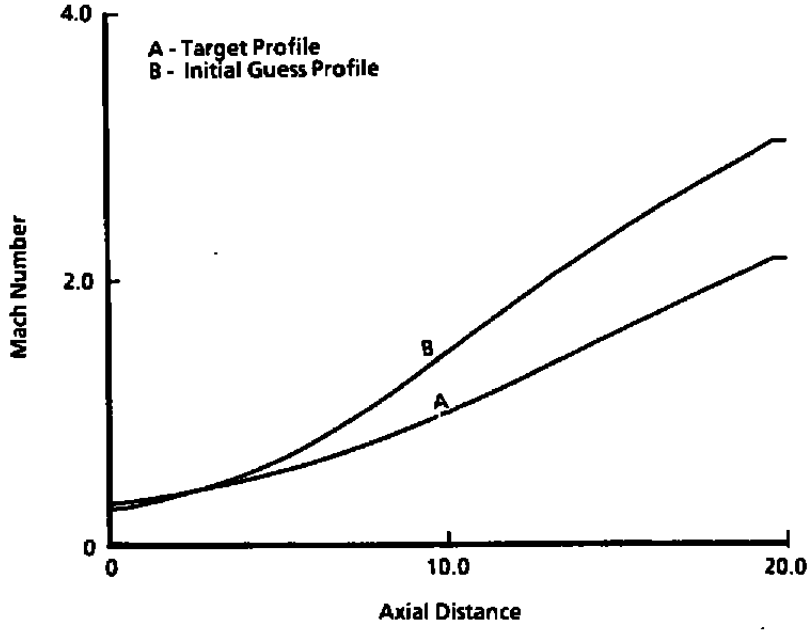

Figure 22. Planar convergent/divergent nozzle centerline Mach number distribution.

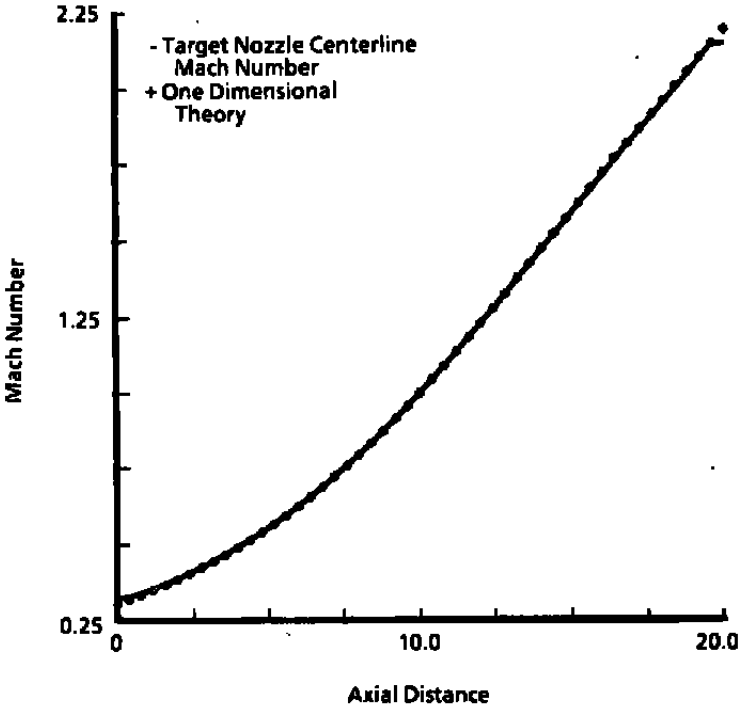

Figure 23. Planar convergent/divergent nozzle centerline Mach number comparison to one-dimensional theory.

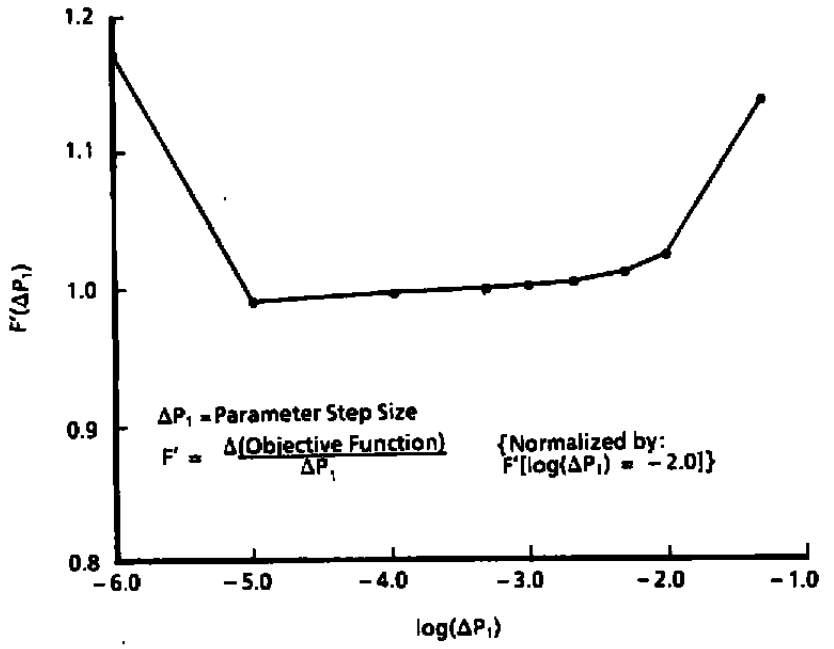

Figure 24. Planar convergent/divergent nozzle objective function derivative sensitivity.

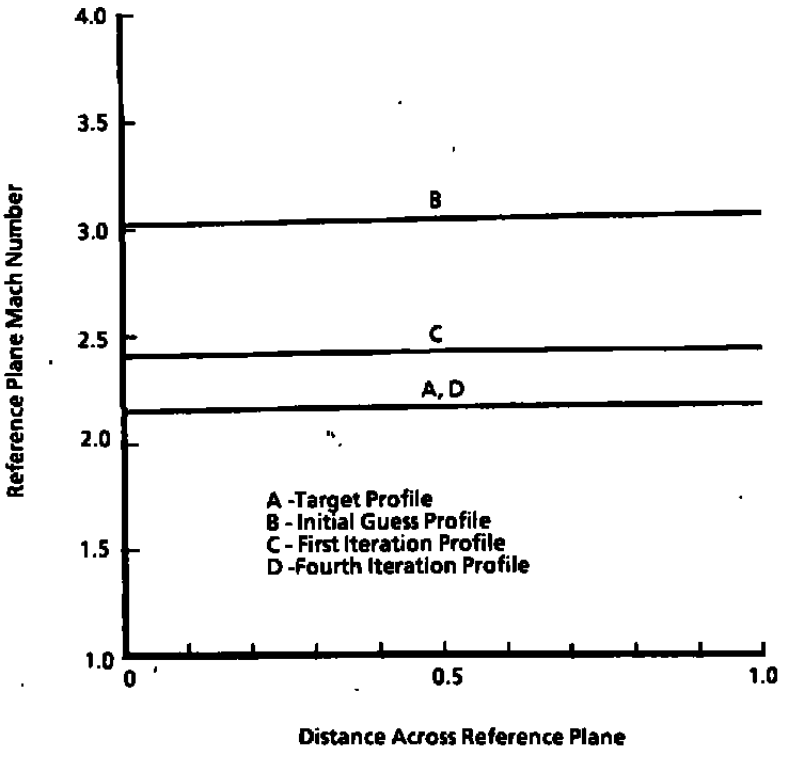

Figure 25. Planar convergent/divergent nozzle RP Mach number profiles.

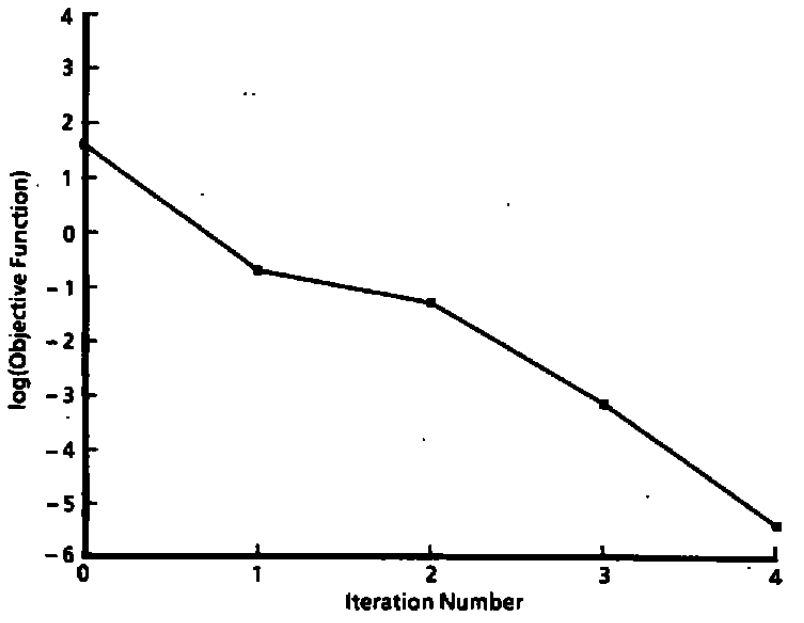

Figure 26. Planar convergent/divergent nozzle objective function reduction.

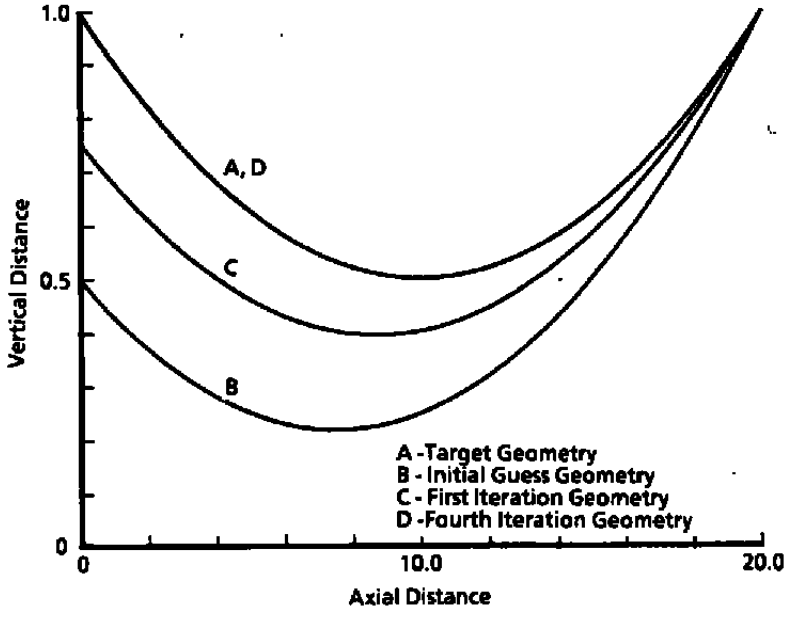

Figure 27. Planar convergent/divergent nozzle wall contour variation.

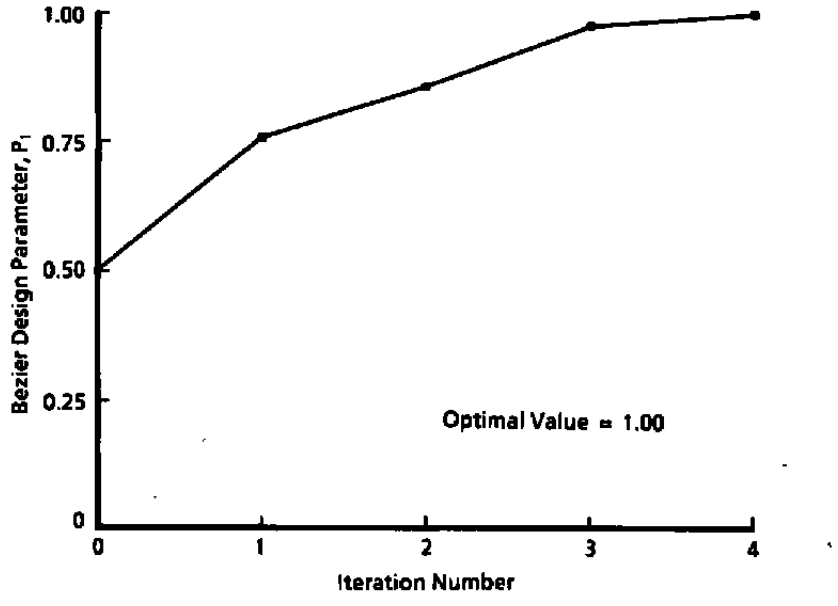

Figure 28. Planar convergent/divergent nozzle Bezier design parameter, P_1, convergence.

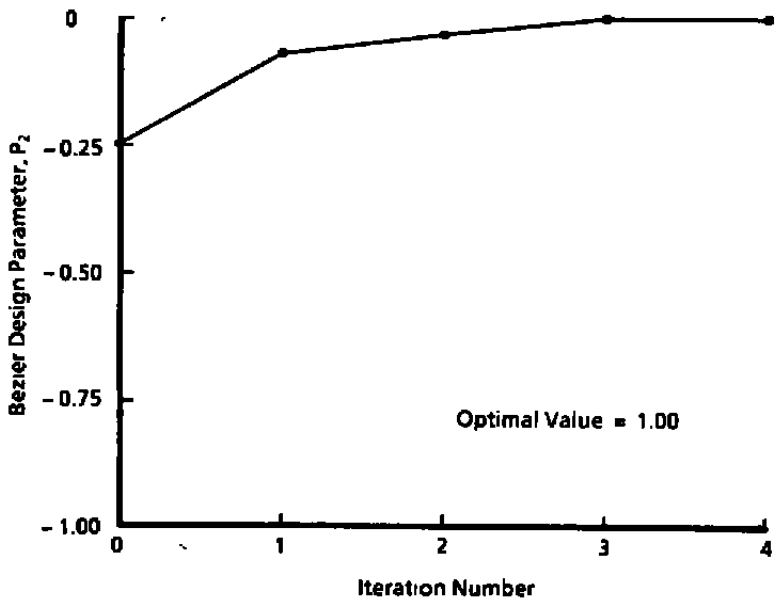

Figure 29. Planar convergent/divergent nozzle Bezier design parameter, P_2, convergence.

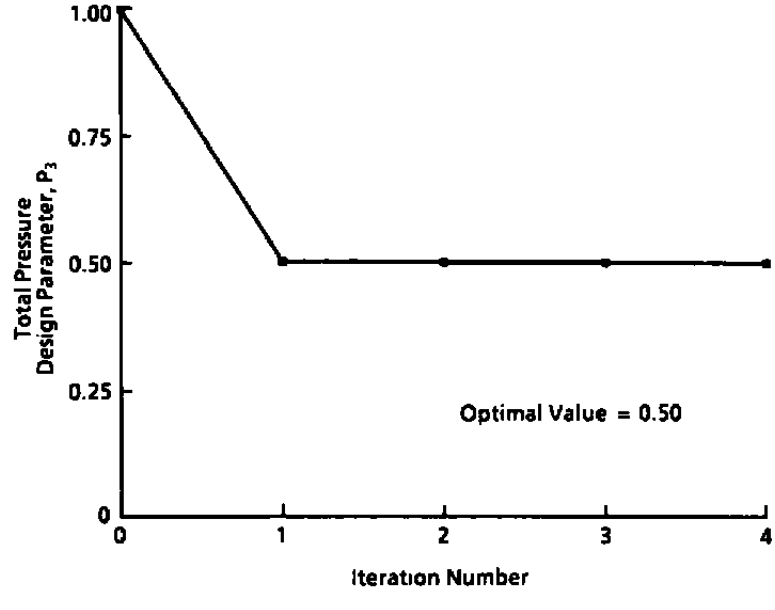

Figure 30. Planar convergent/divergent nozzle total pressure design parameter, P_3, convergence.

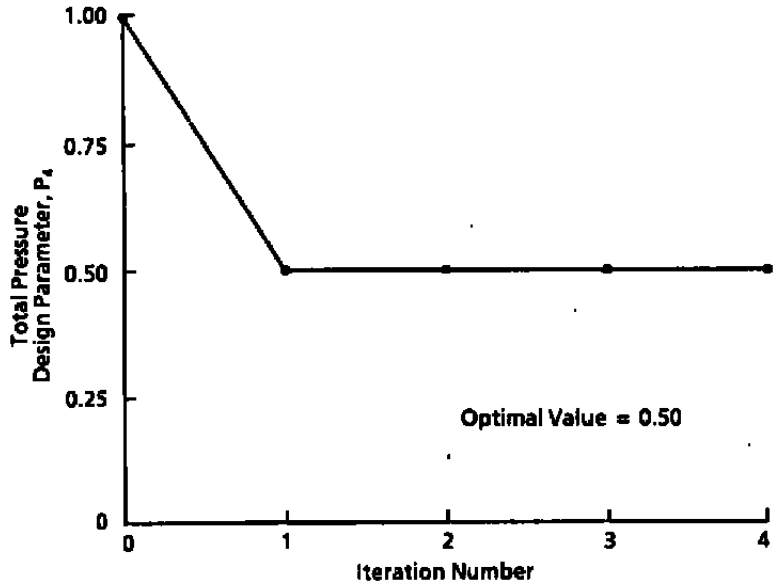

Figure 31. Planar convergent/divergent nozzle total temperature design parameter, P_4, convergence.

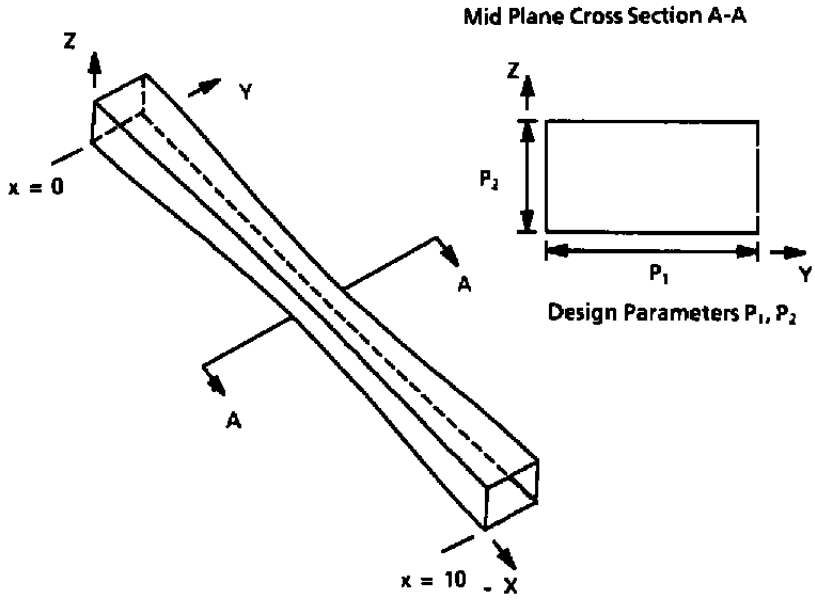

Figure 32. 3-D convergent/divergent nozzle optimization.

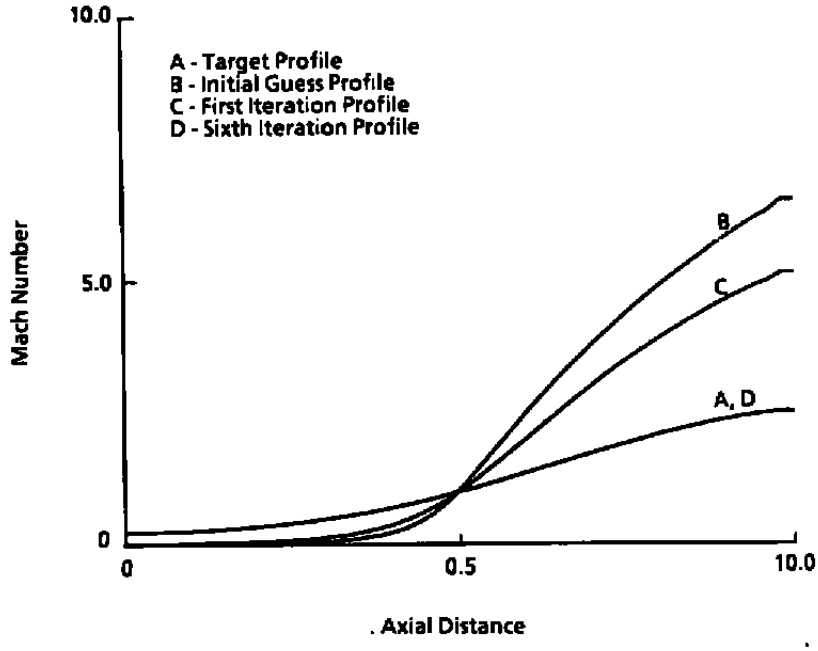

Figure 33. 3-D convergent/divergent nozzle centerline Mach number distribution comparison.

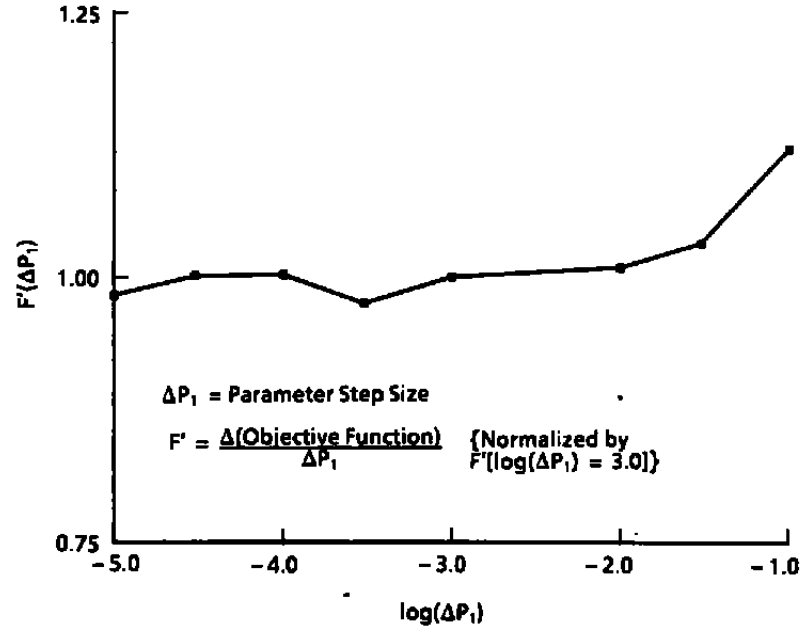

Figure 34. 3-D convergent/divergent nozzle derivative sensitivity.

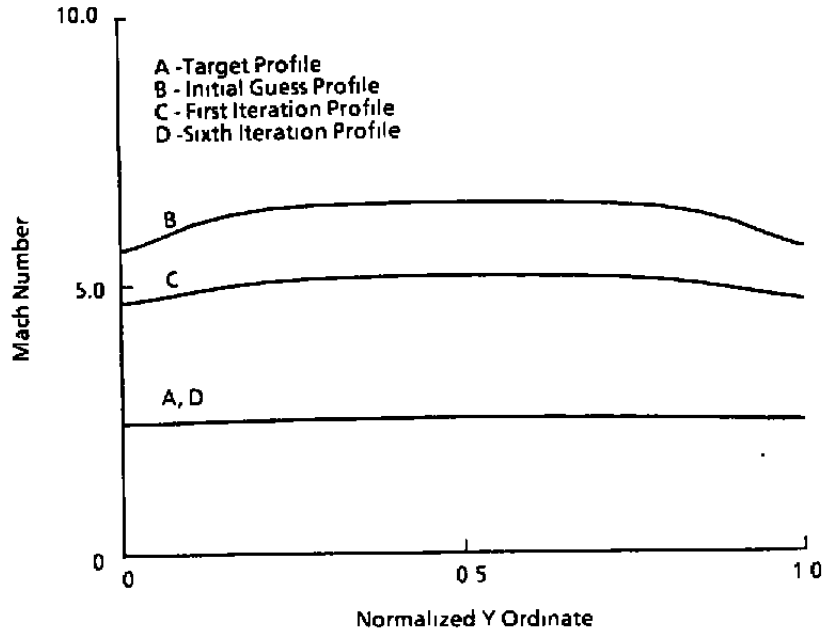

Figure 35. 3-D convergent/divergent nozzle RP Mach number variation (Z = 0).

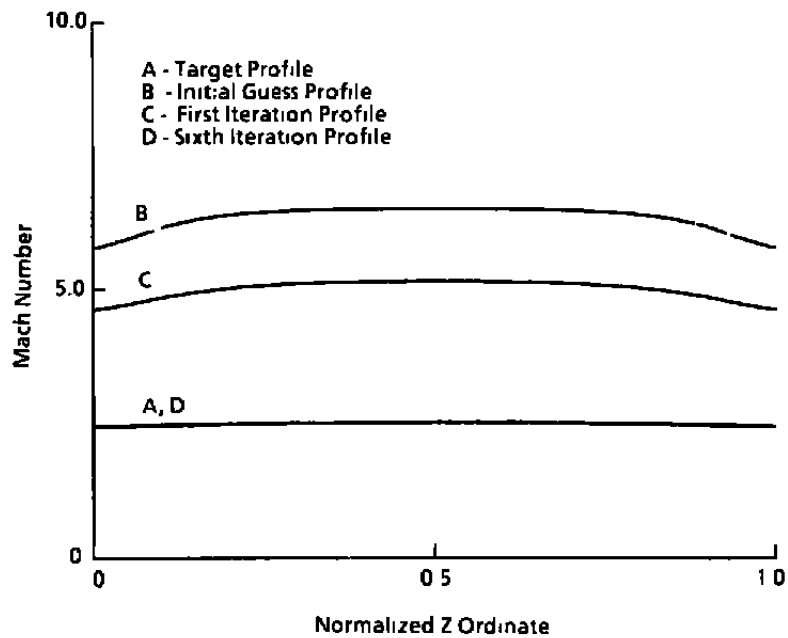

Figure 36. 3-D convergent/divergent nozzle RP Mach number variation (Y = 0).

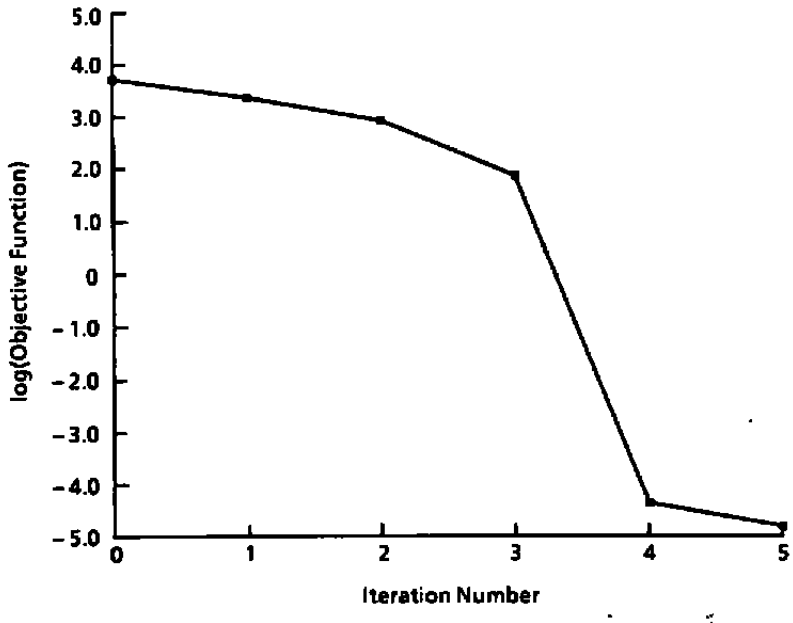

Figure 37. 3-D convergent/divergent nozzle objective function reduction.

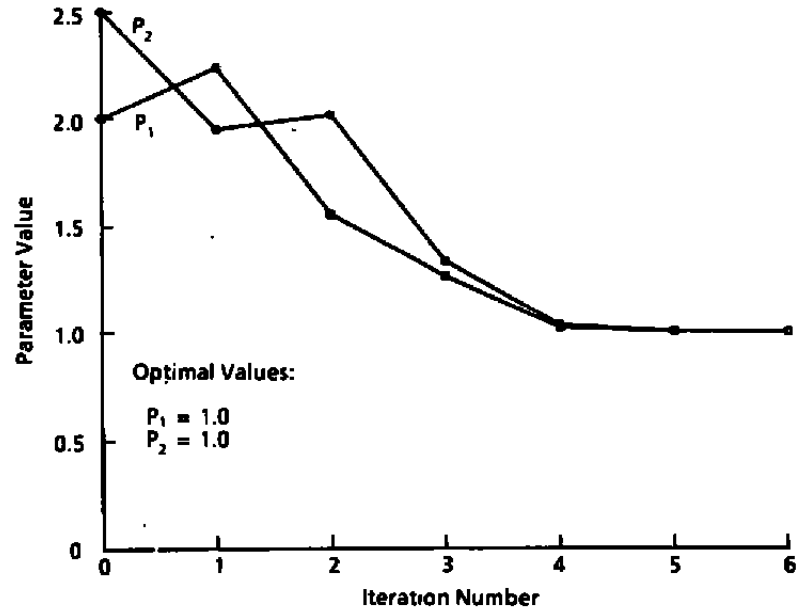

Figure 38. 3-D convergent/divergent nozzle design parameter convergence.

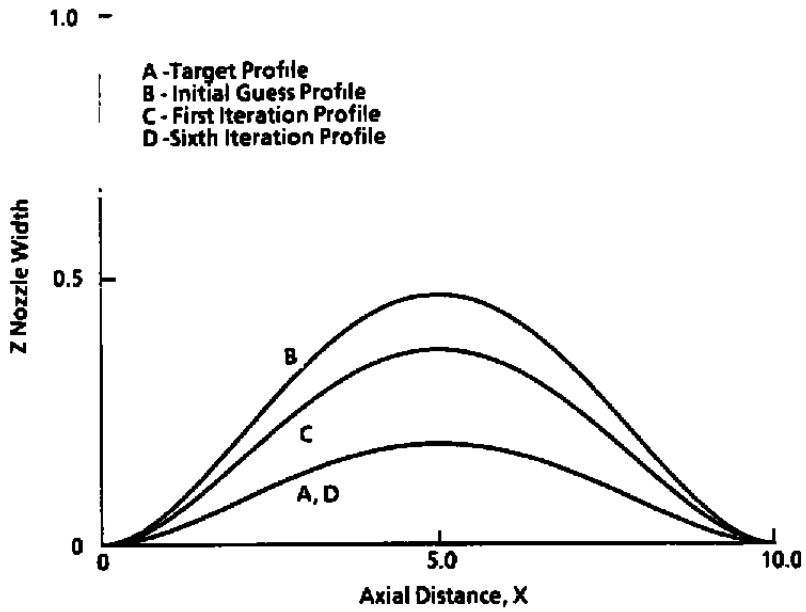

Figure 39. 3-D convergent/divergent nozzle wall contour convergence for constant Y plane.

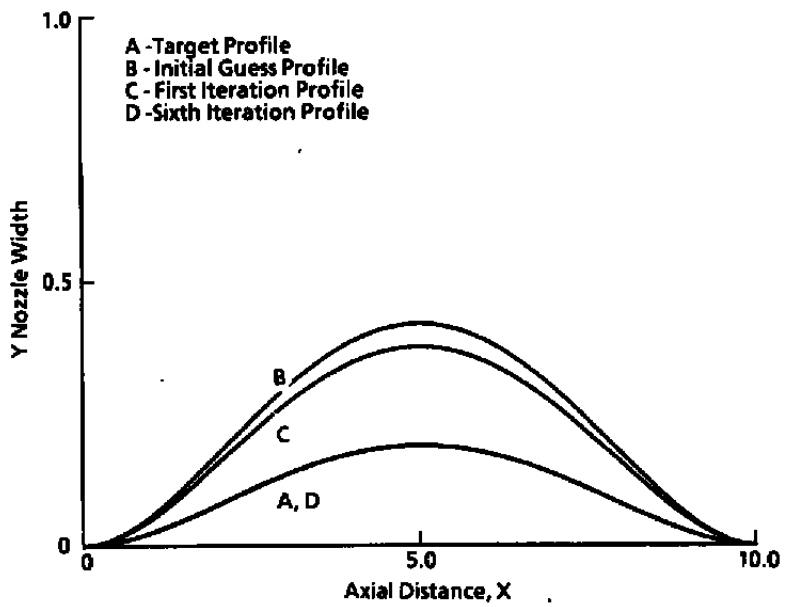

Figure 40. 3-D convergent/divergent nozzle wall contour convergence for constant Z plane.

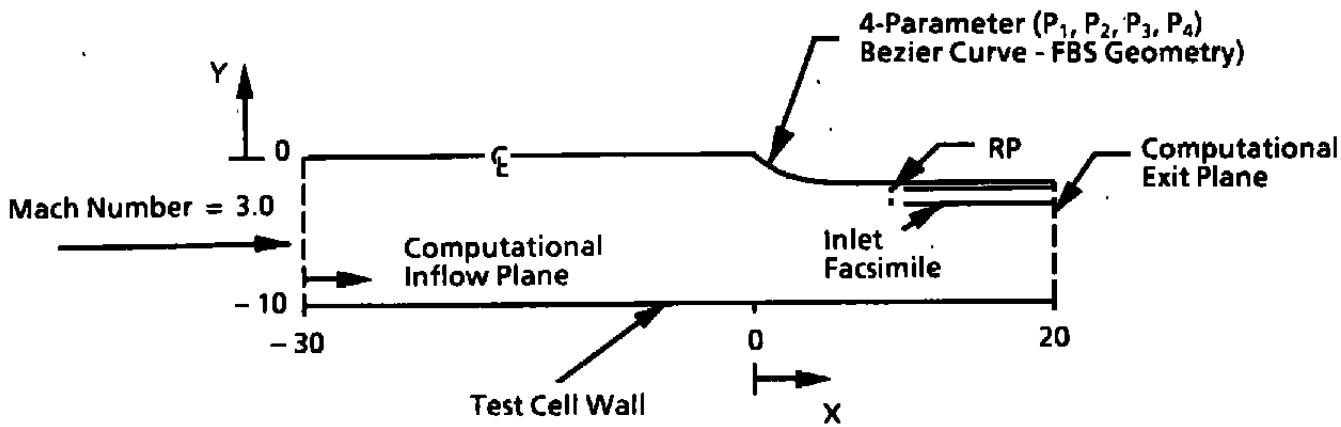

Figure 41. Planar supersonic forebody simulator optimization.

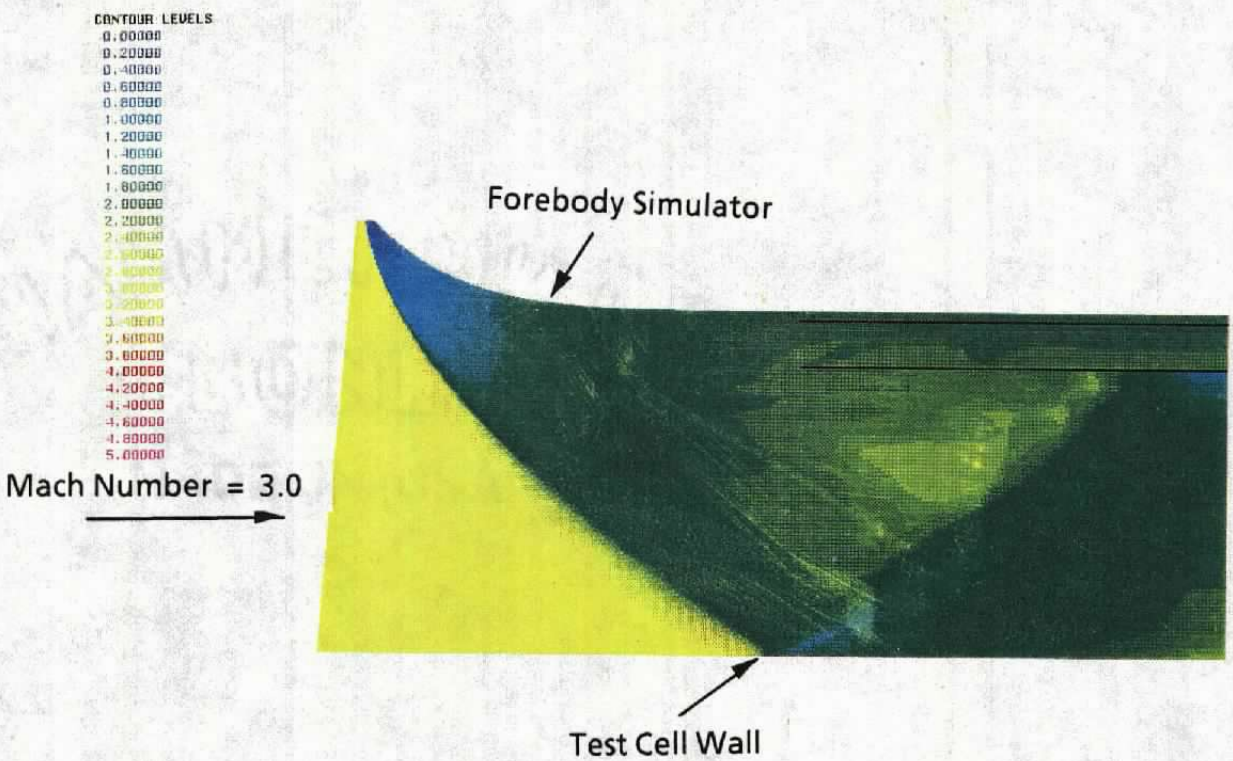

Figure 42. Target design Mach contours in the forebody simulator/inlet region.

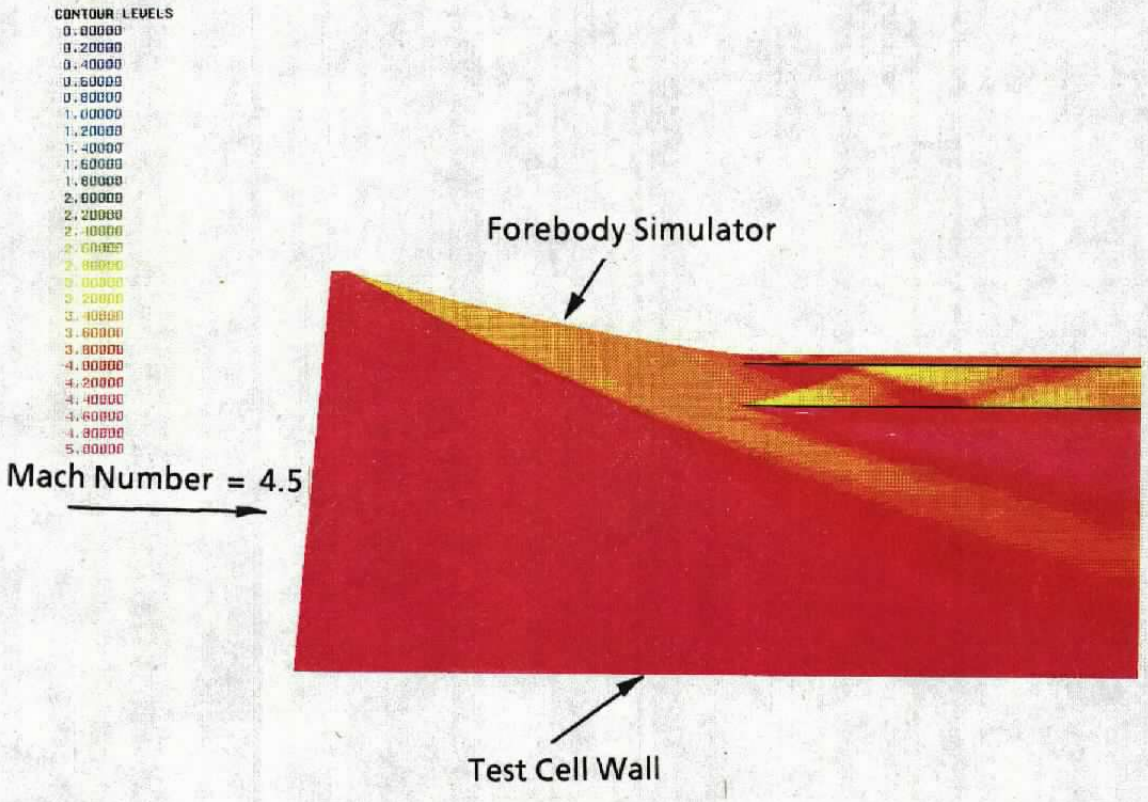

Figure 43. Initial guess Mach contours in the forebody simulator/inlet region.

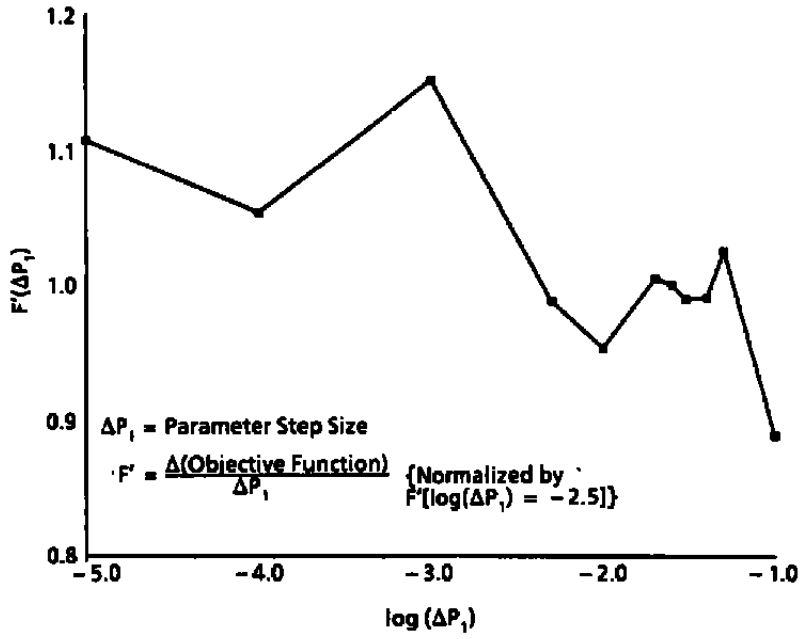

Figure 44. Planar supersonic forebody simulator derivative sensitivity.

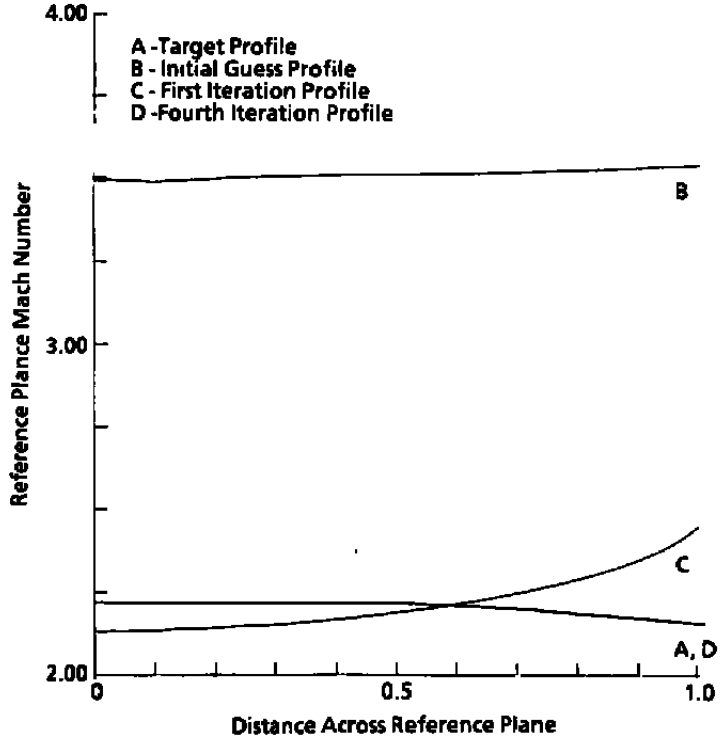

Figure 45. Planar supersonic forebody simulator RP Mach number profiles.

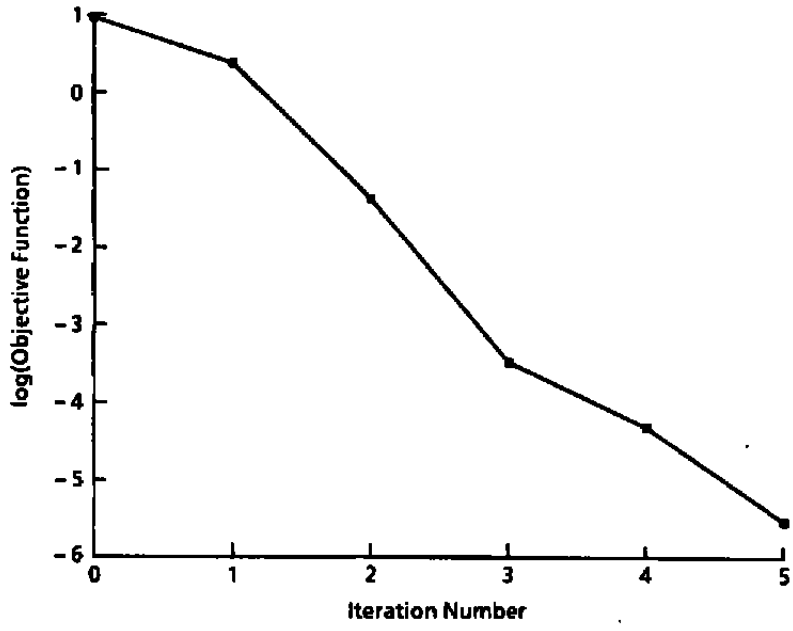

Figure 46. Planar supersonic forebody simulator objective function reduction.

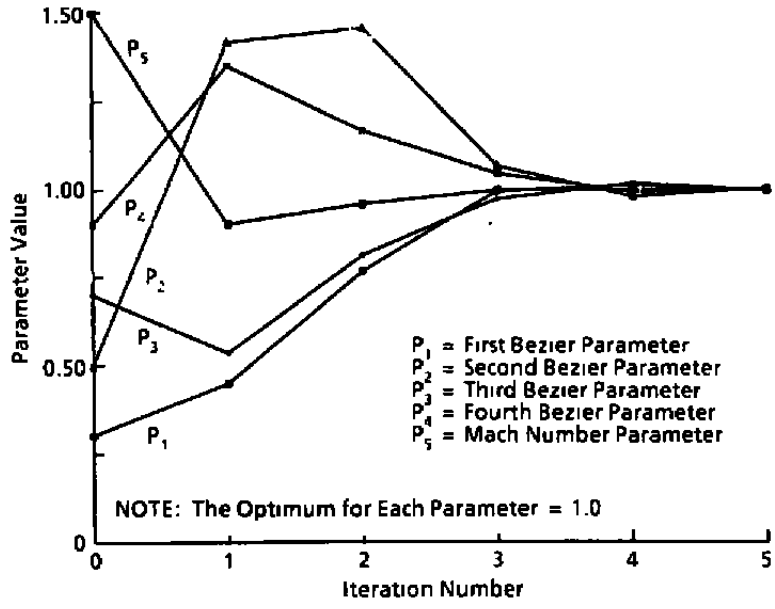

Figure 47. Planar supersonic forebody simulator design parameter convergence.

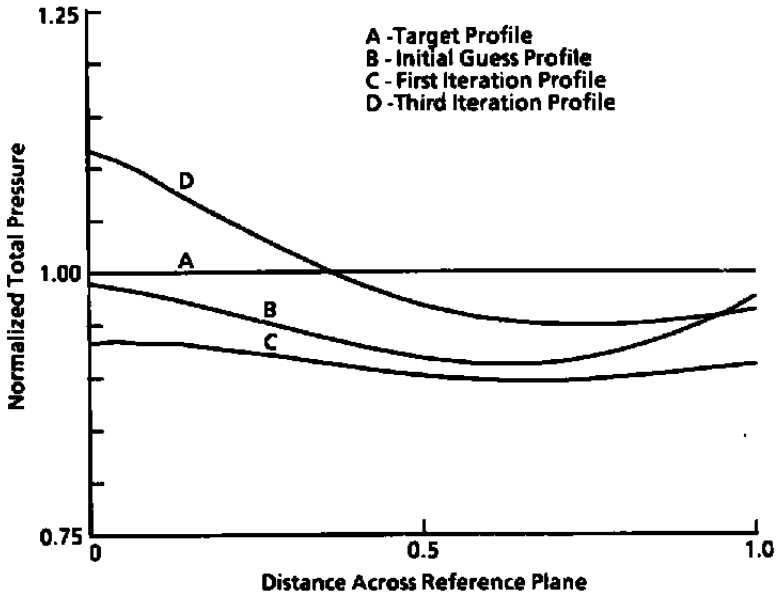

Figure 48. Comparison of the total pressure component of the objective function for a shortened forebody simulator.

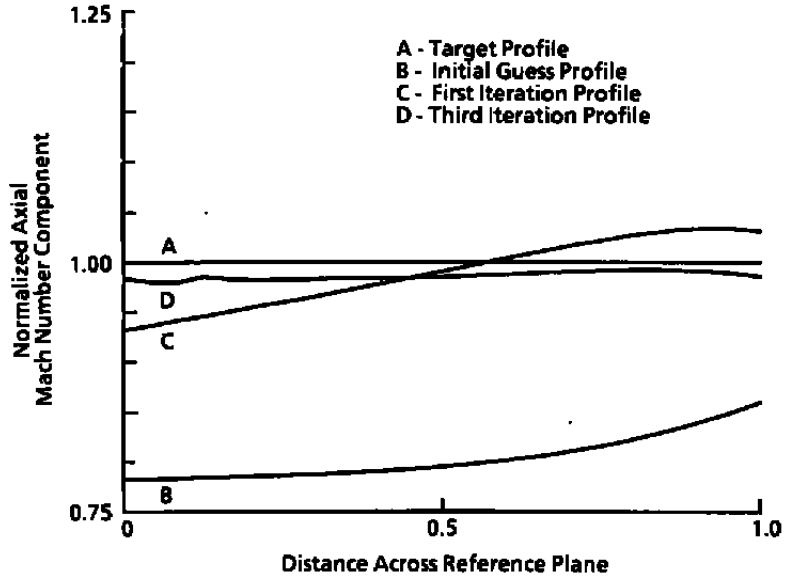

Figure 49. Comparison of the axial Mach number component of the objective function for a shortened forebody simulator.

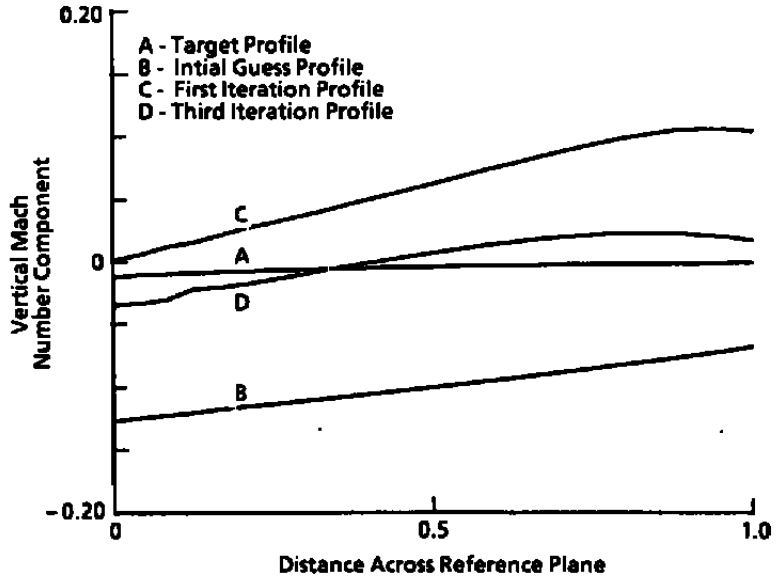

Figure 50. Comparison of the vertical Mach number component of the objective function for a shortened forebody simulator.

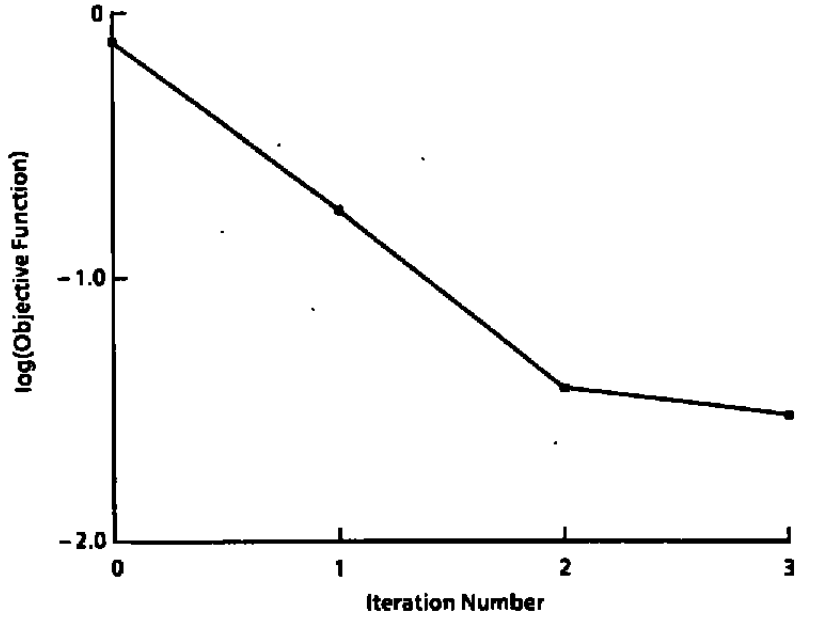

Figure 51. Shortened supersonic forebody simulator objective function reduction.

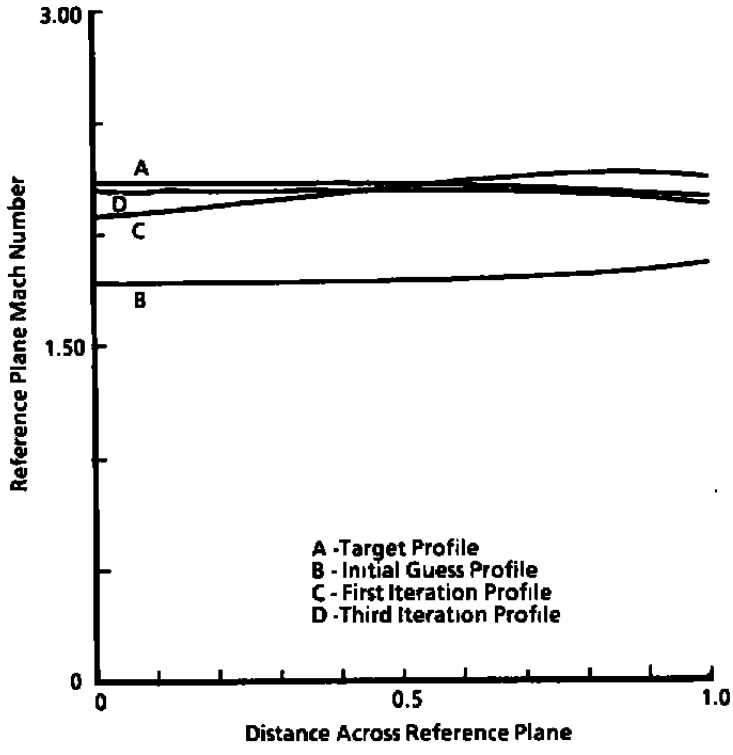

Figure 52. Shortened supersonic forebody simulator RP Mach number profiles.

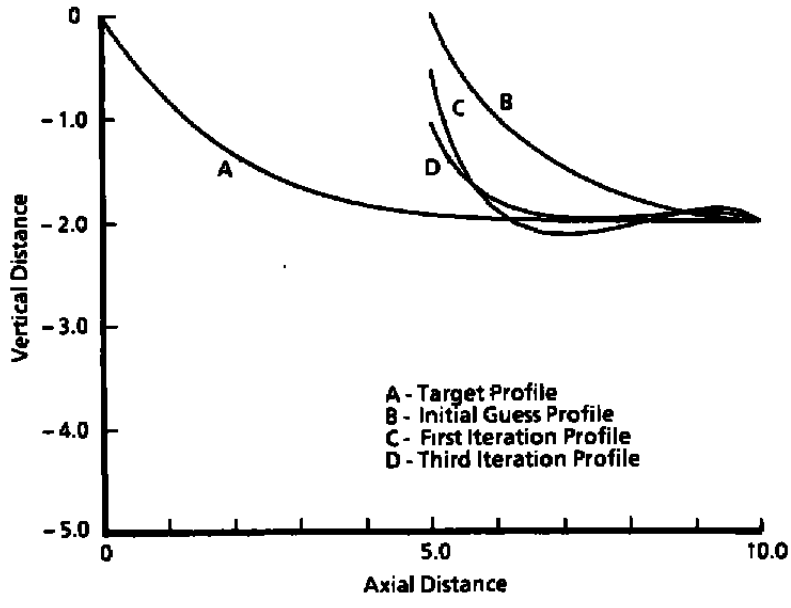

Figure 53. Shortened supersonic forebody simulator variation in variable geometry.

APPENDIX A

GAUSS-NEWTON ALGORITHM

To formulate the nonlinear least-squares minimization algorithm, let the residuals $r_i(P_1,\ldots,P_M)$, $i = 1,2,\ldots,N$, be functions of the M design parameters, $\underline{P}$. To minimize r_i, in the least-squares sense, values for the parameters, P, are found that minimizes

$$F(\underline{P}) = \sum_{i=1}^{N} \{y_i - f_i(\underline{P})\}^2 = \sum_{i=1}^{N} \{r_i(\underline{P})\}^2 \tag{A-1}$$

where y_i denotes the N specified reference plane quantities, and f_i denotes the computed M quantities for the associated design parameters, $\underline{P}$.

The Gauss-Newton minimization algorithm is derived by first substituting a first-order Taylor series expansion about $\underline{P}^0$ into Eq. (A-1) for $r_i(\underline{P})$. This yields

$$F(\underline{P}) \sim \sum_{i=1}^{N} \left\{ r_i(\underline{P}^0) + \sum_{j=1}^{M} \frac{\partial r_i(\underline{P}^0)}{\partial P_j} \Delta P_j \right\}^2 \tag{A-2}$$

with $\Delta\underline{P}_j$ defined as the j^{th} component of the vector

$$\Delta\underline{P} = \underline{P} - \underline{P}^0 \tag{A-3}$$

Minimizing Eq. (A-2) requires

$$\frac{\partial F(\underline{P})}{\partial P_k} = 0 \tag{A-4}$$

for each k. Applying condition, Eq. (A-4), to Eq. (A-2) yields the following system of equations:

$$2 \sum_{i=1}^{N} \left\{ r_i(\underline{P}^0) + \sum_{j=1}^{M} \frac{\partial r_i(\underline{P}^0)}{\partial P_j} \Delta P_j \right\} \frac{\partial r_i(\underline{P}^0)}{\partial P_k} = 0 \tag{A-5}$$

for $k = 1,2,3,\ldots,M$. Rearranging (A-5)

$$\sum_{i=1}^{N} \left\{ \sum_{j=1}^{M} \frac{\partial r_i(\underline{P}^0)}{\partial P_j} \Delta P_j \right\} \frac{\partial r_i(\underline{P}^0)}{\partial P_k} = - \sum_{i=1}^{N} \left\{ r_i(\underline{P}^0) \frac{\partial r_i(\underline{P}^0)}{\partial P_k} \right\} \tag{A-6}$$

Defining J as the Jacobian matrix of the residual vector, $\underline{R}$, with respect to the parameter vector, $\underline{P}$, allows the M equations defined by Eq. (A-6) to be written more concisely in vector notation as

$$J^T J\Delta\underline{P} = - J^T\underline{R} \qquad \text{(A-7)}$$

where J is defined by Eq. (5). This M-by-M system of equations is then solved to determine the parameter corrections at each iteration.

APPENDIX B

BROYDEN'S JACOBIAN UPDATE FORMULA

Application of the Gauss-Newton optimization algorithm requires solution of the system of equations,

$$J^T J \Delta \underline{P} = - J^T \underline{R} \tag{B-1}$$

where $\underline{R}$ denotes the residual vector of length N, $\underline{P}$ denotes the parameter vector of length M, $\Delta \underline{P}$ denotes the computed change in parameters, and J denotes the Jacobian matrix of $\underline{R}$ with respect to $\underline{P}$. Equation (B-1) then determines a search vector, $\Delta \underline{P}$, and a linear search can be carried out so that

$$\underline{P}_{k+1} = \underline{P}_k + \nu \Delta \underline{P}_k \tag{B-2}$$

where ν is selected to reduce the norm of $\underline{R}_{k+1}$ sufficiently below the norm of $\underline{R}_k$. Eliminating the linear search is equivalent to specifying $\nu = 1$ in Eq. (B-2).

A quasi-Newton method is derived by assuming at the k^{th} iteration a current design point, $\underline{P}_k$, and an approximation, B_k, to J_k has been obtained. The Jacobian initial value, B_0, can be computed by a finite difference approximation. The first-order Taylor series expansion of $\underline{R}_{k+1}$ gives

$$\underline{R}_{k+1} = \underline{R}_k + J_k \Delta \underline{P}_k \tag{B-3}$$

or in terms of the Jacobian approximation, B_k,

$$B_k \Delta \underline{P}_k = \Delta \underline{R}_k \tag{B-4}$$

A method is sought to approximate B_{k+1} without reapplying a finite difference representation. The method introduced by Broyden (Refs. 12 and 14), requires that B_{k+1} satisfy the quasi-Newton condition,

$$B_{k+1} \Delta \underline{P}_k = \Delta \underline{R}_k \tag{B-5}$$

which provides N equations for the N × M unknown elements of B_{k+1} in Eq. (B-5). This is motivated by examining the behavior when $\underline{R}$ is linear. For linear $\underline{R}$ Eq. (B-5) constrains B_{k+1} to hold exact derivative information in the direction of $\Delta \underline{P}_k$. This is apparent from Eq. (B-3), which is exact for linear $\underline{R}$. The additional N × (M − 1) equations are obtained by

requiring the change in $\underline{R}$ predicted by B_{k+1} in all directions orthogonal to $\Delta\underline{P}_k$, to be the same as would be predicted by B_k. Symbolically, that provides

$$B_{k+1}\underline{q}_i = B_k\underline{q}_i \tag{B-6}$$

where the $\underline{q}_i$ form a basis in the $(M-1)$ dimensional subspace orthogonal to $\Delta\underline{P}_k$. Thus,

$$\Delta\underline{P}_k^T\underline{q}_i = 0 \tag{B-7}$$

for each of the $M-1$ directions, $\underline{q}_i$. Define Q to be a matrix of vectors so that

$$Q = (\Delta\underline{P}_k \quad \underline{q}_1 \quad \underline{q}_2 \cdots \underline{q}_{(M-1)}) \tag{B-8}$$

For convenience select the length of $\underline{q}_i$ as

$$\underline{q}_i^T\,\underline{q}_i = \Delta\underline{P}_k^T\Delta\underline{P}_k \tag{B-9}$$

Now

$$Q^TQ = (\Delta\underline{P}_k^T\Delta\underline{P}_k)I \tag{B-10}$$

which yields

$$Q^{-1} = \frac{Q^T}{\Delta\underline{P}_k^T\Delta\underline{P}_k} \tag{B-11}$$

Combining Eq. (B-8) with Eq. (B-6) gives

$$B_{k+1}Q = B_kQ + (B_{k+1}\Delta\underline{P}_k - B_k\Delta\underline{P}_k)\underline{M} \tag{B-12}$$

where

$$\underline{M} = (1\ 0\ 0\ \ldots\ 0) \tag{B-13}$$

Combining Eq. (B-5) with Eq. (B-12) gives

$$B_{k+1}Q = B_kQ + (\Delta\underline{R}_k - B_k\Delta\underline{P}_k)\,\underline{M} \tag{B-14}$$

Post multiplying by Q^{-1} gives

$$B_{k+1} = B_k + (\Delta\underline{R}_k - B_k\Delta\underline{P}_k)\underline{M}\,Q^{-1} \tag{B-15}$$

Substituting from Eq. (B-11) gives

$$B_{k+1} = B_k + \frac{(\Delta\underline{R}_k - B_k\Delta\underline{P}_k)\underline{M}\,Q^T}{\Delta\underline{P}_k^T\Delta\underline{P}_k} \tag{B-16}$$

which upon simplification gives

$$B_{k+1} = B_k + \frac{(\Delta\underline{R}_k - B_k\Delta\underline{P}_k)\Delta\underline{P}_k^T}{\Delta\underline{P}_k^T\Delta\underline{P}_k} \tag{B-17}$$

APPENDIX C

QUADRATIC INTERPOLATION LINEAR SEARCH

Following Hartley (Ref. 13), let F_0 denote the objective function value for the initial value of the solution vector, $\underline{P}^0$, of a Gauss-Newton or quasi-Newton iteration. Let F_1 denote the objective function value at the updated value of the solution vector, $\underline{P}^1$, where $\underline{P}^1$ is given by

$$\underline{P}^1 = \underline{P}^0 + \Delta\underline{P} \tag{C-1}$$

with $\Delta\underline{P}$ denoting the computed correction to the solution vector for the optimization iteration. Let ν define a variable so that $\nu = 0$ at $\underline{P}^0$ and $\nu = 1$ at $\underline{P}^1$. The objective function can now be approximated in the interval (0,1) by an interpolation function with the optimization value analytically determined. In particular, if the objective function is evaluated at $\nu = m$, within the interval, then $F(\underline{P}^0 + \nu\Delta\underline{P})$ can be approximated by a quadratic function of the form

$$f(\nu) = p\nu^2 + q\nu + r \tag{C-2}$$

If F_m satisfies the criterion

$$F_m < F_0 \tag{C-13}$$

and

$$F_m < F_1 \tag{C-4}$$

then a minimum of $f(\nu)$ must exist in the interval (0,1). Differentiating Eq. (C-2) with respect to ν^* and setting the result equal to zero yields

$$\nu^* = -\frac{q}{2p} \tag{C-5}$$

with ν^* denoting the location of the minimum of $F(\nu)$ in the interval. The system of equations

$$\begin{pmatrix} 0 & 0 & 1 \\ 1 & 1 & 1 \\ m^2 & m & 1 \end{pmatrix} \begin{pmatrix} p \\ q \\ r \end{pmatrix} = \begin{pmatrix} F_0 \\ F_1 \\ F_m \end{pmatrix}$$

is solved to determine the coefficients p, q, and r of the quadratic. Substituting these coefficients into Eq. (C-5) yields

$$\nu^* = \frac{1}{2} \frac{(1 - m^2) F_0 + m^2 F_1 - F_m}{(1 - m) F_0 + m F_1 - F_m} \tag{C-7}$$

The functional value $f(\nu^*)$ should then be a better approximation to the minimum than F_1, which resulted from the optimization algorithm. Because of the expense of function evaluations within this research, the described line search was only used when the optimization algorithm failed to produce a reduction in functional value. Symbolically, if $F_1 > F_0$, then the line search was used. A similar quadratic line search method can be derived for the interval by using F_0, F_1, and the $f'(0)$. Since $f'(0)$ is computed to implement the optimization algorithm, this approach eliminates the need for the evaluation of F_m. This implementation was not evaluated herein.

NOMENCLATURE

B	Jacobian approximation
C_1	First algebraic test function convergence criterion
C_2	Second algebraic test function convergence criterion
F	Least-squares objective function
$g_i^P(u)$	Bernstein basis function defined by Eq. (10)
J	Jacobian matrix of $\underline{R}$ with respect to $\underline{P}$ defined by Eq. (5)
M	Total number of design parameters
M_x	Mach number component along the x axis
M_y	Mach number component along the y axis
M_z	Mach number component along the z axis
N	Total number of residual components
N_r	Number of reference plane points
N_c	Number of parameter constraints
$\underline{P}$	Design parameter vector
P_i	Individual design parameter
P_T	Total pressure
r_i	Least-squares residual component
$\underline{R}$	Residual component vector
RP	Aerodynamic optimization reference plane

t	NACA0012 airfoil thickness parameter [See Eq. (11)]
T_T	Total temperature
u	Bernstein-Bezier interpolation parameter [See Eqs. (8) and (9)]
v	Bernstein-Bezier interpolation parameter [See Eq. (9)]
w	Bernstein-Bezier interpolation parameter [See Eq. (9)]
x	NACA0012 airfoil axial coordinate [See Eq. (11)]
$\underline{x}_i$	Position vectors of Bezier control points [See Eq. (8)]
$\underline{x}_{ijk}$	Position vectors of 3-D Bezier control points [See Eq. (9)]
$\underline{x}(u)$	Bernstein-Bezier polynomial [See Eq. (8)]
$\underline{x}(u,v,w)$	3-D Bezier polynomial [See Eq. (9)]
$y(x)$	Function used to define NACA0012 airfoil [See Eq. (11)]
$\Delta\underline{P}$	Computed change in design parameter vector P